Bulletin of Earthquake Engineering (2022) 20:6129–6165
https://doi.org/10.1007/s10518-022-01436-6

ORIGINAL ARTICLE

Response of reinforced mortar-less interlocking brick wall under seismic loading

Guanyu Xie[1] · Xihong Zhang[1] · Hong Hao[1] · Kaiming Bi[1] · Yuanzheng Lin[2,3]

Received: 11 August 2021 / Accepted: 21 May 2022 / Published online: 12 June 2022

Abstract
Mortar-less construction with interlocking bricks has many advantages, such as improved construction efficiency and relatively low requirements on labour skills. Nevertheless, the seismic performance of interlocking brick structures is not well understood yet. In this paper, laboratory tests and numerical modelling are carried out to investigate the seismic behaviour of interlocking brick walls. Laboratory shaking table tests are performed on a scaled reinforced mortar-less interlocking brick wall. The response and damage modes under in-plane seismic loading are investigated. A detailed numerical model is then generated and validated with the laboratory testing data. Unlike the conventional masonry wall that diagonal shear damage governs the failure, the interlocking brick wall exhibits rocking responses, whose damage is mainly at the two bottom corners of the wall. Full-scale interlocking brick walls are then modelled and compared with conventional concrete masonry unit (CMU) walls bonded by mortar. Comparisons are made between the seismic resistances and damage modes of the two walls. The influences of ground motion intensities, vertical components of seismic excitations and different seismic time histories on the seismic behaviour of the interlocking brick wall are examined. It is found that the interlocking brick wall has a higher seismic resistance capacity than the conventional CMU wall. Inter-brick friction is the main energy dissipation mechanism in the interlocking brick wall. Because of the rocking response, vertical component of the ground motion significantly influences the damage of interlocking brick wall. The interlocking brick wall is insensitive to velocity pulses of ground motions due to its relatively high natural frequency.

Keywords Interlocking brick · Seismic · Mortar-less · Rocking · Shaking table test

✉ Xihong Zhang
xihong.zhang@curtin.edu.au

[1] Centre for Infrastructural Monitoring and Protection, School of Civil and Mechanical Engineering, Curtin University, Bentley, WA 6102, Australia

[2] Engineering Research Centre of Safety and Protection of Explosion and Impact of Ministry of Education (ERCSPEIME), Southeast University, Nanjing 211189, Jiangsu, China

[3] School of Civil Engineering, Southeast University, Nanjing 211189, Jiangsu, China

1 Introduction

Masonry structure is one of the oldest structure forms and is still widely used all over the world due to its outstanding fire resistance, thermal and sound insulation performances, and relatively low cost. Nevertheless, compared to reinforced concrete and steel structures, masonry structures are relatively weak against extreme loadings such as earthquake due to their low ductility, high specific weight, and weak connection between bricks (Lourenço et al. 2013; Tomaževič 1999). Therefore, damages and even collapses of masonry structures are always reported in the wake of earthquakes. For instance, in the 2008 Wenchuan Earthquake, 50% of the masonry structures in the epicentre area completely collapsed (Sun et al. 2008). Although in Australia the seismicity is low to moderate, hazards from earthquakes on structures still exist due to widespread masonry structures, which have poor seismic resistance (Maqsood et al. 2016). For example, in the 1968 Meckering Earthquake, a number of masonry buildings were extensively damaged, some of which completely collapsed (Kateiva 1970; Smith 1969) (Fig. 1a). In the 1989 Newcastle Earthquake, despite the low earthquake intensity, over 10,000 buildings suffered modest to substantial damages, most of which were masonry structures or non-structural masonry components (Page 1991, 2019) (Fig. 1b). In the 2010 Kalgoorlie-Boulder earthquake, some old masonry structures and modern masonry residential buildings suffered structural damages (Edwards et al. 2010; Wehner et al. 2010) (Fig. 1c). Therefore, it is necessary to properly analyse and design masonry structures against earthquake loading for people and property protection.

1.1 Interlocking bricks

Recently, mortar-less masonry structures using interlocking bricks have attracted much attention in the construction industry (Sturm et al. 2015; Wang et al. 2017). Ramamurthy and Kunhanandan Nambiar (2004) carried out a review on masonry structures constructed with interlocking bricks and demonstrated the construction efficiency of using interlocking brick could be significantly improved compared to that of conventional bricks. Peirs (1998) found the labour requirement could be reduced by 65% by using interlocking bricks. Additionally, the construction quality of masonry structures using interlocking bricks can be improved and the requirement on labour skills could be substantially reduced as the interlocking mechanism of bricks can help ensure alignment, robustness and strength requirements (Ali et al. 2012; Wang et al. 2017). Moreover, interlocking bricks could provide a higher mechanical efficiency factor (structure equivalent compressive strength over brick unit compressive strength) due to the elimination of mortar bed joints, which

(a) Meckering, 1968 (Central Wheatbelt Visitor Centre 2016) **(b)** Newcastle, 1989 (Rawling 2012) **(c)** Kalgoorlie, 2010 (Wehner et al. 2010)

Fig. 1 Damage of masonry structures in earthquakes

significantly improves the compressive performance of masonry structures (Ramamurthy and Kunhanandan Nambiar 2004). The factor is around 0.3–0.4 (Ramamurthy and Kunhanandan Nambiar 2004) for conventional brick structures, while mortar-less interlocking brick structures could provide up to 0.96 (Ali et al. 2012; Hendry 1998). With all those advantages, various types of interlocking bricks have been developed which feature with different interlocking mechanisms and therefore different mechanical performances (Anand and Ramamurthy 2000, 2005; Haener 1987; Bosro et al. 2018; Shi et al. 2021a; Thanoon et al. 2004). As the design of interlocking shapes can be regarded as an optimisation problem, digital tools have been employed. For example, Casapulla et al. (2019) developed a digital framework to quantify and minimise the sliding infeasibility of dry-stacking interlocking structures. Different materials have also been used to make interlocking bricks, such as rammed earth blocks, rice husk ash cement blocks, and coconut fibre reinforced concrete, whose mechanical performances are reported by different researchers (Al-Fakih et al. 2018; Ali and Chouw 2013; Fay et al. 2014; Oyebisi 2018).

Interlocking bricks are connected through the interlocking tenons and mortises instead of relatively weak mortar as in conventional bricks, whose shear strength can be assimilated the bond strength between mortar and masonry units in conventional mortared masonry (Casapulla et al. 2021). As pointed out by some researchers (Casapulla et al. 2019; Shi et al. 2021b; Dyskin et al. 2012), interlocking brick structures exhibit high shear resistances on the inter-brick interfaces. For instance, Sturm et al. (Sturm et al. 2015) conducted shear tests on dry-stack interlocking rammed earth blocks, and demonstrated the effectiveness of the relatively shallow extrusion on the block in improving the brick shear strength. As friction plays an important role in mortar-less masonry structures, Liu et al. (2016) investigated the frictional resistance between stacked interlocking bricks of different shapes and found that the frictional coefficients gradually degrade under cyclic loading. It is worth noting that most existing interlocking bricks have relatively small shear keys mainly for alignment in construction (Anand and Ramamurthy 2000, 2005; Haener 1987; Bosro et al. 2018; Thanoon et al. 2004), which therefore could only provide limited shear resistance. It has been demonstrated that segmental concrete columns with large shear keys have improved shear resistance compared to the ones without shear keys or with only small keys under both static and dynamic loading conditions (Zhang et al. 2017, 2018, 2021). Accordingly, The shear capacity as well as the seismic capacity of interlocking bricks could possibly be improved by introducing larger and properly designed shear keys to the bricks, which has not been explicitly and well studied yet. Another unique feature of dry-stacked interlocking structures is that the damage of one brick is usually confined to this brick itself and will not propagate to adjacent bricks. Oikonomopoulou et al. (2018) tested dry-stacking interlocking glass piers, in which cracks developed in the glass block but stopped at the interlocking joint without extending into the adjacent blocks. Consequently, the interlocking glass pier did not fail in a brittle manner. Furthermore, the absence of mortar between bricks enables friction at the brick interfaces, which could increase the energy dissipation capacity of a structure under earthquake actions (Ali et al. 2013). The seismic behaviour of interlocking brick structures would differ from that of a conventional masonry structure. More systematic study is needed to properly understand the earthquake behaviour of interlocking brick structures.

1.2 Seismic research on interlocking brick masonry structures

Numerous studies have been conducted to investigate the seismic responses of conventional brick structures (Ahmed et al. 2017; Ferreira et al. 2015; Ferretti and Pascale 2019; Gupta and Sankhla 2018; Magenes and PENNA 2011), but only very limited research is available in the open literature on the seismic resistance performance of interlocking brick structures. Under seismic excitation, masonry piers made of conventional bricks usually fail with shear-dominant response mode (Peña et al. 2010; Sucuoglu and McNiven 1991). This is because the shear resistance of mortar joints is relatively low. In contrast, piers made of interlocking bricks are expected to have a higher shear resistance capacity because the interlocking mechanism could provide more shear resistance. Similarly, for conventional masonry walls subjected to in-plane ground excitation, diagonal and direct shear failures along mortar joints are usually observed (Magenes and Calvi 1997). In comparison, the interlocking brick wall could respond differently because of the higher shear resistance (Xie et al. 2020). Qu et al. (2015) investigated the dynamic response of a masonry wall made of interlocking brick featured with two shallow truncated cones. Damages to the tenons were widely observed, indicating the influence of the interlocking mechanism. Furthermore, gap opening could be developed on mortar-less brick structures, which may influence the responses of masonry structures under earthquake loading. Elvin and Uzoegbo (2011) carried out shaking table tests on a full-scale dry-stacked (mortar-less) masonry structure and observed significant gap opening during the test. Ali et al. (2013) also conducted shaking table tests on brick piers and walls made of interlocking blocks. Brick uplifting was observed during the test, which indicated a flexure-dominated response mode. These laboratory tests mentioned above provide insights into the behaviour of interlocking brick structures, but there is still no systematic study yet on the response of interlocking brick structures, as well as damage and failure criteria under earthquake loading. Furthermore, interlocking keys of different interlocking bricks were designed differently. Since interlocking key is the primary factor that provides shear resistance, masonry structures constructed with interlocking bricks of different keys perform differently. It is necessary to understand the mechanism and performance of interlocking keys in resisting seismic ground excitations of masonry structures.

In earthquake design, the energy dissipation capacity of a structure is a major concern. Plastic hinges are typically formed in reinforced masonry piers/walls made of conventional bricks, which consume most energy when the structure suffers substantial damage. Because of the mortar-less construction method, joint openings could occur due to rocking response, which avoids the formation of plastic hinge. When rocking happens, the kinetic energy will be dissipated through collisions between adjacent blocks (Housner 1963; Magenes and Calvi 1997; Priestley et al. 1978; Sorrentino et al. 2011). Therefore, the hysteretic energy dissipation capacity of masonry structures made of interlocking bricks could be very different from that of conventional bricks. Qu et al. (2015) carried out cyclic tests on interlocking brick walls. It was found that the hysteretic curves were stable and showed a lower strength and stiffness degradation even at a high drift ratio. It also showed a stable energy dissipation capacity through the whole process and the interlocking brick wall exhibited a flexure-dominated response mode. Again, there is still no comprehensive study yet about the energy dissipation performance of interlocking brick structures under earthquake excitation.

This study examines the seismic behaviour of masonry walls made of interlocking bricks constructed with the mortar-less method. Shaking table tests are firstly carried out; then, a detailed numerical model is generated and validated with the laboratory testing data. The seismic response of the interlocking brick wall is analysed in terms of the response and damage modes, seismic resistance, and energy dissipation mechanism. Comparison between the interlocking brick wall and a conventional CMU wall on their seismic performance is carried out. The influences of the vertical component and velocity pulses of seismic excitations on the seismic behaviour of the interlocking brick walls are also examined.

2 Laboratory shaking table test

2.1 Details of interlocking bricks

Figure 2a illustrates the interlocking bricks used in this study. They are designed with large tenons and mortises that interlock with neighbouring blocks, which help to improve the shear resistance capacity of the interlocking wall. Moreover, as the structure is constructed using the mortar-less method, inter-brick sliding and local oscillation could occur if some interlocking keys are damaged under heavy loading (Bland 2011), which would dissipate imposed energy through friction and movements of bricks. For the scaled shaking table test, half-scale bricks are cast with dimensions illustrated from different aspects

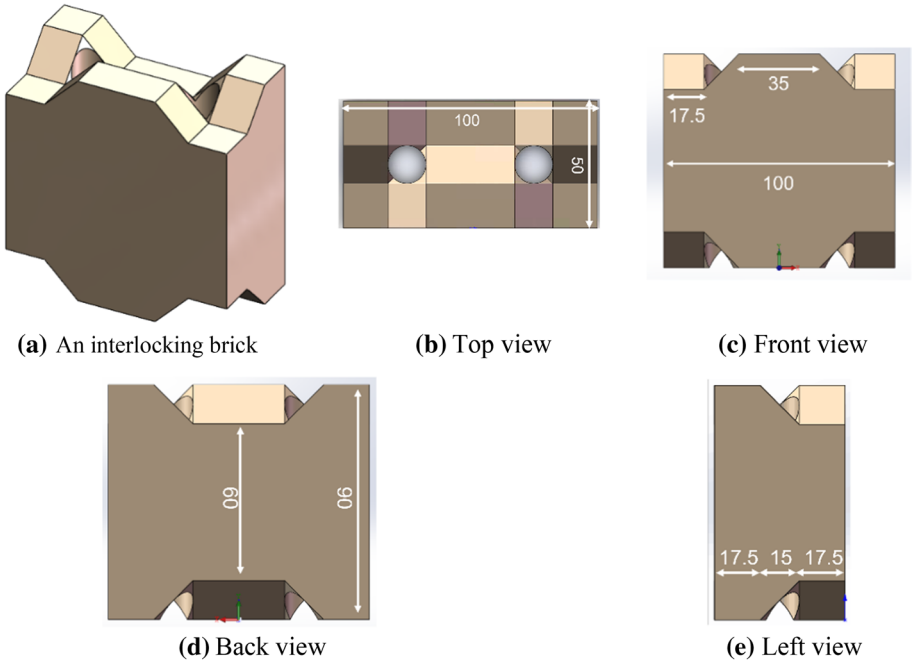

(a) An interlocking brick **(b)** Top view **(c)** Front view

(d) Back view **(e)** Left view

Fig. 2 Geometry and dimension of the half-scale interlocking bricks (unit: mm)

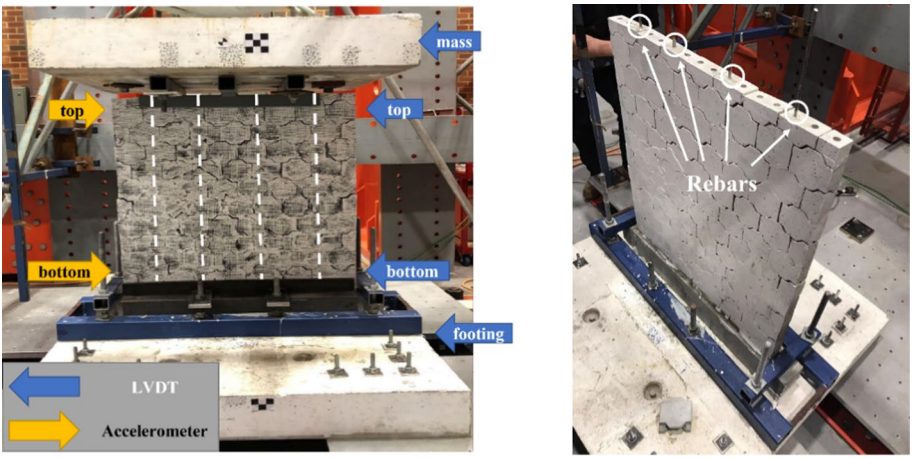

(a) Elevation view of the wall **(b)** Distribution of reinforcement

Fig. 3 Setup of interlocking brick wall for the shaking table test

in Fig. 2b–e. The material used for making these bricks has a characteristic compressive strength of 17.5 MPa.

2.2 Wall setup and instrumentation

As shown in Fig. 3a, a scaled brick wall of 825 mm tall and 800 mm wide comprising 12 tiers of interlocking bricks is built for the shaking table tests. Four pieces of 6 mm-diameter ribbed bars are grouted into the holes of the interlocking bricks to reinforce the wall at approximately equal spacing, as marked and highlighted in Fig. 3b (0.3% vertical reinforcement ratio). It is to note that due to the wall width and hole distribution in the brick, strict equal spacing of the rebars could not be achieved, but the distance between the outer rebars and the wall side is maintained the same at 125 mm. A 375 kg solid concrete block is placed on top of the wall to apply a vertical load of 0.1 MPa.

Four 1 m × 1 m shaking tables in the Structural Dynamics Laboratory of Curtin University are rigidly connected using a concrete slab and synchronised as one biaxial shaking table for this test. The payload of each shaking table is 8kN and the operating frequency is 0.1–50 Hz. The four shaking tables are able to simulate spatially varying ground motions with sinusoidal or random waveforms. In this test, the seismic loading is applied in the in-plane horizontal direction of the wall.

Four accelerometers are installed onto the specimen wall, i.e., on the top mass (named as “Mass”), at the top of the wall (named as “Top”), at the bottom of the wall (named as “Bottom”), and at the middle of the footing (named as “Footing”), respectively. Two linear variable differential transducers (LVDTs) are installed to monitor the in-plane horizontal displacements of the wall. One is installed at the top of the wall (named “Top”), and the other is installed to measure the bottom displacement of the wall (named “Bottom”). The sensors are connected to an HBM® data logging system, synchronised and sampling at a frequency of 300 Hz. Only uniaxial ground motion in the in-plane direction is applied in the tests.

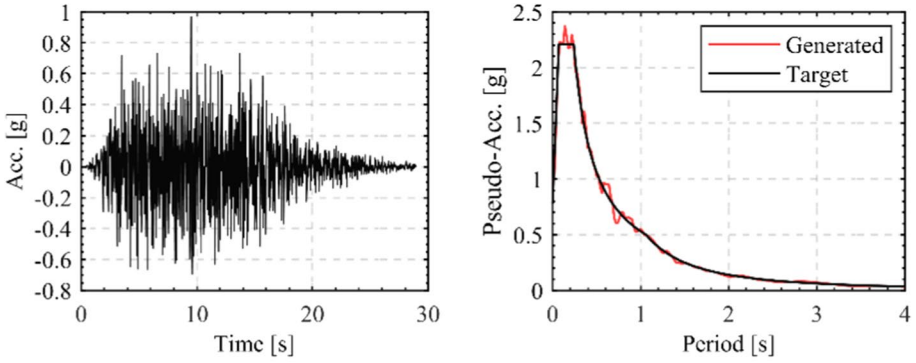

(a) The generated acceleration time history

(b) The elastic response spectra (damping ratio = 5%)

Fig. 4 A typical input with a nominal PGA of 0.6 g

2.3 Test procedures

A synthetic ground acceleration time history complying with Australian seismic design code AS1170.4 (Joint Standards Australia/Standard New Zealand Committee BD-006, General Design Requirements and Loading on Structures 2007) (class C) is generated using the spectral representation method (Bi and Hao 2012) and adopted as the seismic input in this test. The earthquake wave lasts about 30 s. Figure 4a shows a typical acceleration time history with a nominal PGA of 0.6 g generated based on the design response spectra in AS1170.4-2007. The response spectrum of the generated seismic acceleration time history with a 5% damping ratio is shown in Fig. 4b, together with the target spectrum. In the laboratory test, the Peak Ground Acceleration (PGA) of the inputted ground motion time history is gradually increased from 0.05 to 0.6 g. White noise is applied after each ground excitation to examine the frequency of the tested wall so as to check its damage level in terms of the stiffness loss after each ground excitation. It should be noted that, the PGAs here refer to the nominal PGA, namely the scale factor for the standard response spectrum used in the generation of the seismic acceleration time history. Inevitably, there are differences between the nominal PGAs and the actual PGAs of generated seismic ground motion time history used as input in the shaking table tests, as commonly observed in stochastic simulations since the simulated time history is a single realisation of a random process, whereas the PGA used in the simulation represents the mean peak values of the random process. It should also be noted that the shaking table used in the tests is displacement controlled, therefore the actual PGAs on the shaking table is not exactly the same as the input PGAs. The nominal PGAs, the PGAs of the simulated time histories, and those measured at the footing during tests are listed in Table 1.

Table 1 Relationship between nominal PGA, inputted PGA and measured footing PGA

Nominal PGA	0.05 g	0.10 g	0.20 g	0.30 g	0.40 g	0.50 g	0.60 g
Inputted PGA	0.08 g	0.16 g	0.32 g	0.48 g	0.64 g	0.81 g	0.97 g
Measured PGA at footing	0.13 g	0.24 g	0.42 g	0.77 g	0.83 g	0.95 g	1.53 g

3 Numerical modelling

A detailed three-dimensional finite element model of the mortar-less interlocking brick wall is generated using the commercial software Abaqus (Hibbitt et al. 2019). The numerical model is validated with the laboratory shaking table test by comparing the damage modes and the displacement time histories. It is then used to perform numerical simulations to investigate and understand the seismic response of the interlocking brick wall.

3.1 Modelling details

Figure 5a illustrates the numerical model which comprises the top mass, the interlocking brick wall (including the bricks, the rebars and the grouts around the rebars) and the footing. The positions of the four rebars are marked with red dashed lines. Both the interlocking bricks and the grout around the rebars are modelled with three-dimensional solid elements. The rebars, on the other hand, are modelled with beam elements which share the same nodes with the grout surrounding them. The element type C3D8R in Abaqus, namely the continuum stress/displacement three-dimensional eight-node reduced-integration element, is chosen for the solid element. The enhanced hourglass control is enabled to eliminate possible hourglass influence. It is a refinement of the pure stiffness hourglass control method and provides more precise displacement solutions than other common hourglass control approaches such as stiffness control and viscous control (Dassault Systèmes 2022). The element type B31, namely the spatial linear beam element based on the Timoshenko beam theory, is adopted for the beam elements constituting the rebars. A mesh size of 6 mm (shown in Fig. 5b–f for the bricks of different views) is used for the interlocking bricks, the grout and the rebars after a convergence study. In this way, the different parts of the wall in contact with each other have coincident node positions and the contact analysis will have a good accuracy (Dassault Systèmes 2022). The node position coincidence between the grout and the bricks is shown in Fig. 2g, while the rebar elements are generated using the stringer technique and hence share the same nodes as the grout elements surrounding them (Dassault Systèmes 2022). It should be noted that for a better mesh quality, the cylindrical holes in the bricks shown in Fig. 2b are simplified into square holes whose side length equals to the diameter of the round holes. As no intensive local damage was observed around the holes in the test, this simplification has a minimum influence on the simulation results.

3.2 Material model

The concrete damaged plasticity (CDP) model is employed for the brick material. The CDP model is characterised by isotropic tensile and compressive behaviour and progressive damage of material, which can simulate the behaviour of quasi-brittle materials (such as concrete, rock, ceramics and mortar) under cyclic or dynamic loading conditions (Dassault Systèmes 2022; Lubliner et al. 1989). It has been popularly employed in the simulation of concrete and rock structure, and has been used in a recent study on the performance of interlocking bricks with good results (Shi et al. 2021).

The unconfined uniaxial compressive strength of the brick material in the CDP model is set to 17.5 MPa as in the laboratory test. The tensile strength is taken as one-tenth of its compressive strength, following previous studies (Martínez et al. 2018; Shi et al. 2021). The Young's

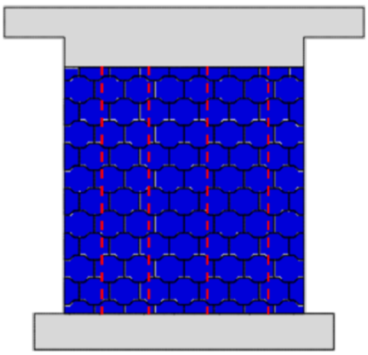

(a) The interlocking brick wall model

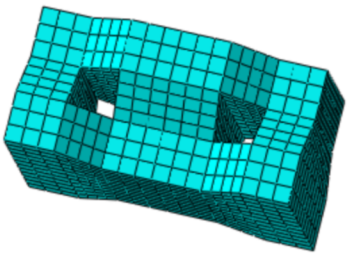

(b) Meshing of one brick

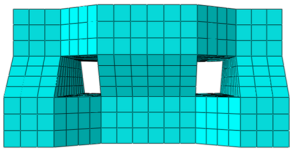

(c) Brick meshing – perspective topview

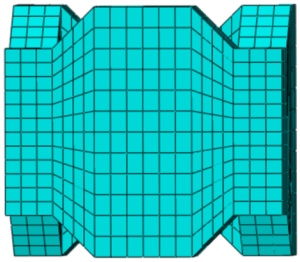

(d) Brick meshing – frontview

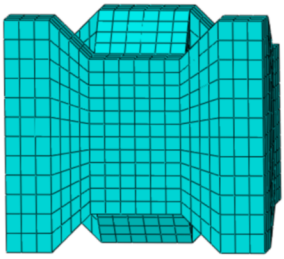

(e) Brick meshing – back view

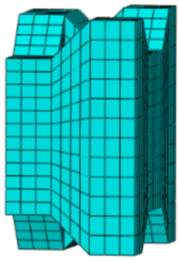

(f) Brick meshing – side view

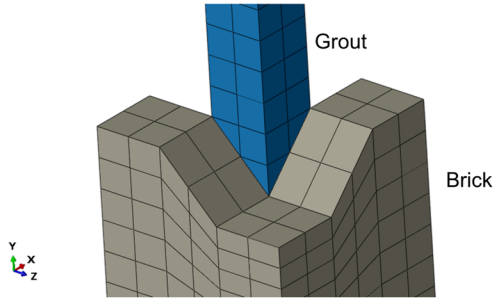

(g) Node position coincidence between the grout and the brick

Fig. 5 Numerical model of the testing wall and its modelling details

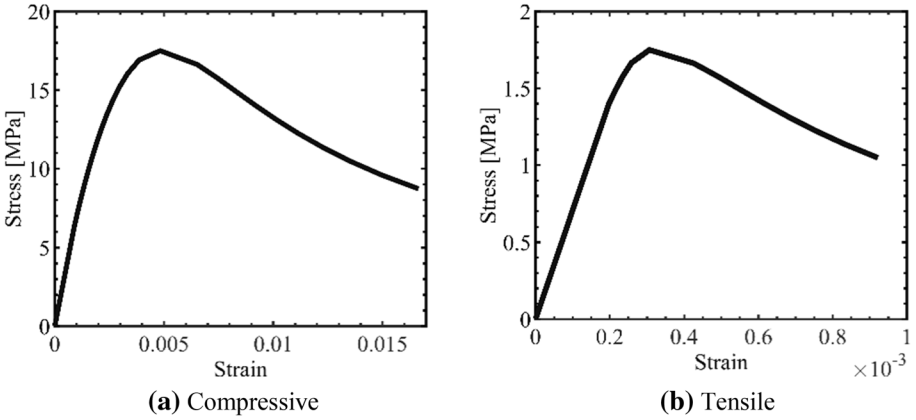

Fig. 6 Stress–strain curves of the brick material

modulus is determined based on 40% of the ultimate compressive strength of the material (Shi et al. 2021). The hardening and softening behaviour of the material is defined following the design code (Minstry of Housing and Urban–Rural Development of the People's of China 2016). The damage parameters are calculated based on strain energy loss using Simpson's integral method (Wang and Yu 2004). The density of the brick material is 2010 kg/m^3; the Poisson's ratio is 0.2; the Young's modulus is 7080 MPa. The compressive and tensile stress–strain relationship of the defined brick material is shown in Fig. 6a, b, respectively. To avoid element tangling, erosion technique is employed (Dassault Systèmes 2022). The scalar unloading stiffness degradation, which is recommended as the damage indicator for materials using the CDP model (Bhartiya et al. 2021; Dassault Systèmes 2022), is adopted to illustrate the damage status in the following sections. An elastic-perfect-plastic material model is used for the steel reinforcement. Table 2 list the material parameters.

3.3 Contacts and analysis steps

For mortar-less constructed interlocking brick wall, properly defining the contact between adjacent interlocking bricks is crucial for accurately modelling of wall responses. In this study, perfect contact between bricks is assumed without considering imperfection. The "hard" contact is set as the contact property in the normal direction. For the tangential direction, a constant friction coefficient of 0.7 is chosen for the interfaces between two contacting bricks (Chen and Bagi 2020). It should be noted that imperfection of bricks inevitably exists, i.e., the brick surface cannot be perfectly smooth. However, in the present study perfect contact between bricks is assumed because there is a lack of data on brick surface roughness, which is randomly distributed and varies from brick to brick, and also because modelling imperfect

Table 2 Material parameters for reinforcement

Density (kg/m^3)	Yield stress (MPa)	Poisson's ratio	Young's modulus (MPa)
7850	500	0.3	206,000

Table 3 Contact setting between the grout and interlocking bricks (Abdulla et al. 2017)

Direction	Stiffness (N/mm^3)	Strength (MPa)	Critical strain energy release rate (N/mm)
Compression	–(*)	17.5	–
Tension	110	0.16	0.012
Shear-first direction	50	0.224	0.05
Shear-second direction	50	0.224	0.05

*Determined by the material of the two contacting surfaces, which is calculated by Abaqus during computation

contact would substantially increase the modelling efforts. Neglecting the imperfect contacts in numerical model would introduce some errors, which should be carefully examined. The infill grout is assumed in perfect contact with the rebars through shared nodes. Cohesive contact is defined between the grout and the bricks, whose parameters are listed in Table 3 following reference (Abdulla et al. 2017). The present model considers that the ribbed reinforcing bars are bonded very well with the grout, while the bonding between the grout and the brick surface is relatively fragile.

The wall is loaded in two stages: firstly, the gravity load is applied to the entire model using dynamic relaxation method (Boulbes 2020). Then, the ground acceleration is applied to the footing to introduce the seismic excitation. Explicit analysis is used in the numerical modelling. Following Eurocode 8 (1998), a damping ratio of 5% is adopted for this wall model. As explicit algorithm is used, the damping is added as a mass proportional damping, calculated based on the in-plane first-order frequency of the wall, while the stiffness proportional damping is neglected to avoid too small stable time increments (Chen et al. 2014; Dassault Systèmes 2022). Following the laboratory test, the numerical model is also subjected to seismic loadings with increasing PGAs to consider the accumulated damage.

4 Results and analysis

The laboratory testing and numerical modelling results are presented in this section. The damage evolution of the interlocking brick wall under gradually increased ground excitation is firstly presented. Localised response in the interlocking bricks is then assessed. The natural frequency of the interlocking brick wall and the wall top displacement time histories under different ground excitations are presented to show the response of the interlocking brick wall under seismic loading. The energy dissipation mechanism is also examined.

4.1 Wall damage evolution

When subjected to 0.05 g and 0.1 g ground excitation, there is no damage observed to the wall. Under 0.2 g seismic loading, apparent inter-brick sliding and local brick oscillation are observed, which originate from pre-existing gaps between interlocking bricks due to inevitable non-perfect contacts between bricks associated with the brick surface roughness (Dell'Endice et al. 2021). After the 0.2 g loading, a significant gap width of 5 mm is observed at the centre of the wall, as shown in Fig. 7a.

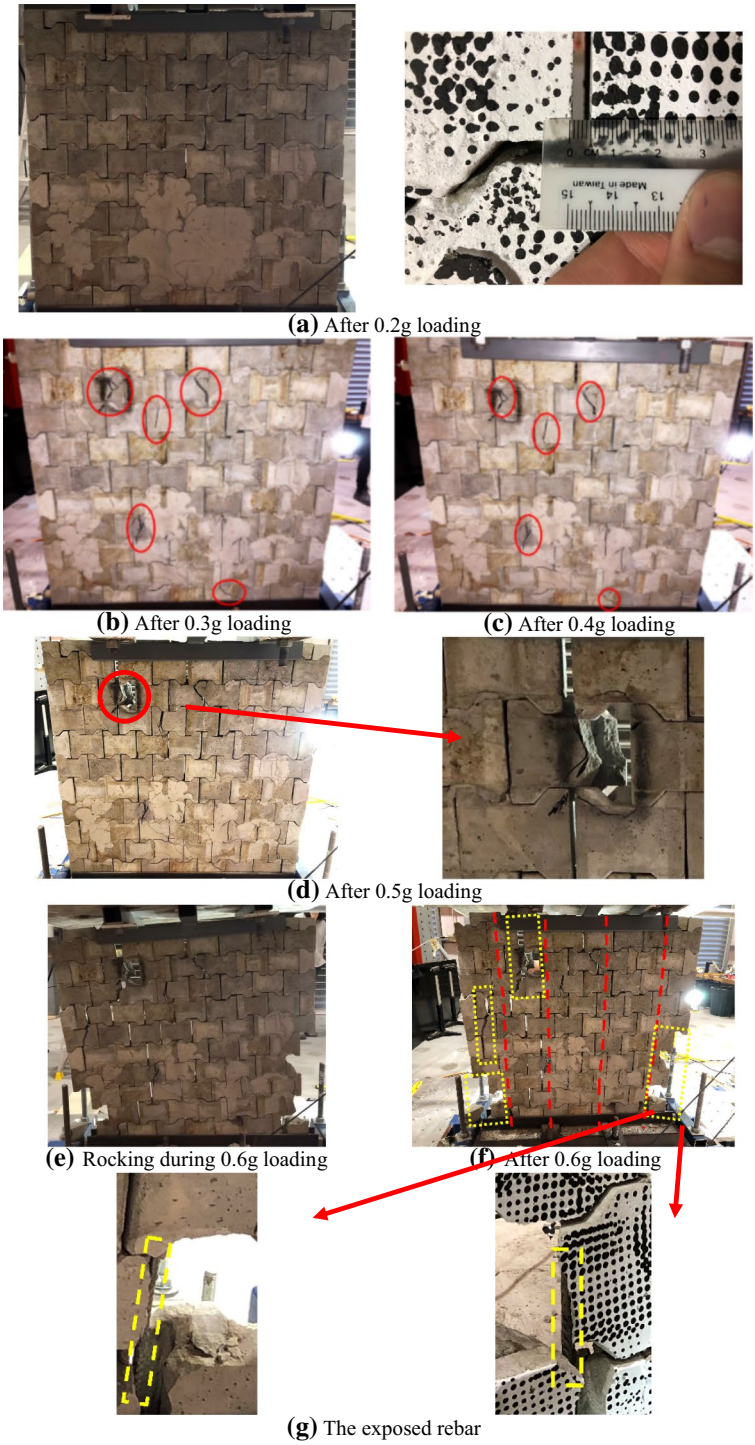

Fig. 7 Progressive wall damages by seismic ground excitations with increasing intensities

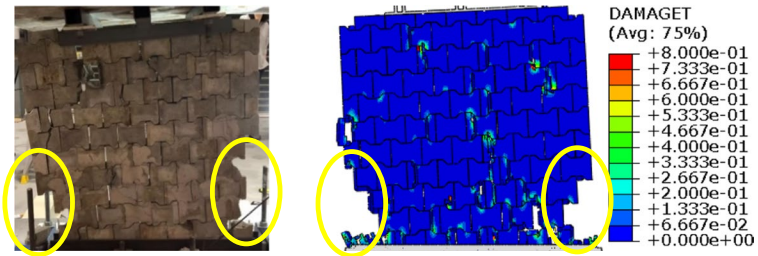

(a) Test **(b)** Simulation

Fig. 8 Comparison of the wall damages under 0.6 g ground excitation between the laboratory test and numerical modelling

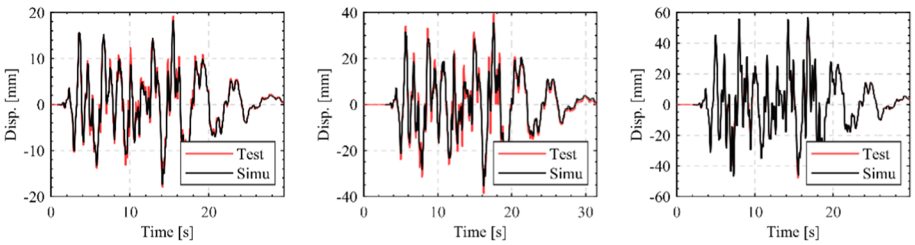

(a) PGA=0.2g **(b)** PGA=0.4g **(c)** PGA=0.5g

Fig. 9 Wall top displacement time histories from the laboratory test and numerical modelling

Under the 0.3 g seismic loading, cracks are initiated in bricks as seen in Fig. 7b, some of which widen and further extend under the 0.4 g loading (Fig. 7c). It is noted that there are no apparent new cracks after the 0.4 g seismic loading compared to the 0.3 g case, signifying the local stress concentration has been released after the formation of those major cracks shown in Fig. 7b, and the wall is in a relatively stable state after the stress redistribution.

Under further increased seismic loading (PGA = 0.5 g), slight rocking responses are observed. With joints opening and closure under the ground excitation, the bricks at the two bottom corners begin to detach during the vibration. More cracks are developed in the interlocking bricks. Moreover, as shown in Fig. 7d, with the widening of gaps in the wall, shattered brick pieces begin to fall off, indicating the damage of the wall. Nevertheless, the wall still manages to hold together and supports the top mass after the 0.5 g excitation. The occurrence of rocking implies that rebar anchorage fails under excessive earthquake loading, which otherwise would have mitigated the formation of rocking (Aslam et al. 1980).

When subjected to the 0.6 g seismic load, severe rocking responses are observed. As shown in Fig. 7e, bricks at the two bottom corners detach because of the successive rocking response, leading to the progressive falling-off of the bricks. Some vertical cracks are formed as a result of the loss of support. Figure 7f shows the severe damage to the wall after this loading case, where the brick damage is highlighted in yellow and the rebar locations in the wall are highlighted in red. As can be observed, despite the severe brick damage, very minor bending deformation is found on the rebars (Fig. 7g). Although the wall still stands, it is deemed to have lost most load-bearing capacity, and the test is hence terminated. Figure 8a, b compare the damage mode of the numerically modelled wall (accumulated damage in previous loading cases are included) with that from the laboratory test

under the 0.6 g ground excitation. It can be found that the numerical model could well reproduce the rocking dominated damage mode of the interlocking brick wall.

4.2 Wall top displacement time histories

Figure 9a–c show the displacement time histories at the top of the wall subjected to ground excitations with different PGAs. Both the laboratory testing and the numerical modelling results are presented here. Since under 0.05 g and 0.1 g excitation, there are no damages in the wall, the displacement time histories are not presented here. Additionally, in the 0.3 g test the LVDT malfunctioned, and in the 0.6 g test the excessive wall rocking response leads to the LVDT out of range. Therefore, the results for these two cases are not compared.

As can be seen, the numerically predicted displacement time histories agree well with those from the laboratory test. Under the PGA = 0.2 g loading, the peak displacement obtained in the test is 19.24 mm, while that from the numerical simulation is 18.31 mm, with an error of 4.83%. In the 0.4 g loading case, the peak displacement responses are 39.75 mm and 35.67 mm respectively from the lab test and numerical modelling, yielding an error of 10.26%. In the 0.5 g case, the interlocking brick wall in the test reaches a peak top displacement of 51.99 mm, while the numerical model predicts a peak displacement of 56.76 mm (+ 9.17% error).

The lateral drift of the wall under different seismic loadings is calculated using the wall top displacement deducting the measured bottom displacement. Table 4 summarises the peak lateral drift ratios in each loading case. As expected, the peak drift ratio gradually increases with the increase in the intensity of input ground excitation. Under the excitation with PGA = 0.4 g, the peak drift ratio is 1.63%, but only minor damage is observed on the tested interlocking brick wall. Both the ASCE 7–16 (Structural Engineering Institute and American Society of Civil Engineers, publisher 2017) and Eurocode 8-2003 (Eurocode 8 1998) specify a 1.0% maximum drift ratio for masonry walls. The present test results indicate the interlocking brick wall can tolerate a higher drift ratio than conventional brick wall as mandated in design codes. The peak drift ratio

Table 4 Summary of shaking table test results

Case	Peak drift ratio	Post-test white noise frequency/ Hz
Before test	–	12.29
PGA = 0.05 g	0.09%	12.28
PGA = 0.1 g	0.22%	12.20
PGA = 0.2 g	0.70%	11.38
PGA = 0.3 g	– *	11.22
PGA = 0.4 g	1.63%	10.54
PGA = 0.5 g	3.42%	8.14
PGA = 0.6 g	– *	–

*1. Under the 0.3 g seismic loading, the bottom displacement time history is not obtained due to malfunction of the LVDT; 2. Under the 0.6 g seismic loading, the wall experiences severe rocking, causing failure of displacement measurement

reaches 3.4% under 0.5 g ground excitation, which is associated with substantial rocking responses of the wall. Nevertheless, the wall still survives this loading cases despite severe damages. It demonstrates the current earthquake design standards for conventional masonry walls, which usually suffer brittle failure under seismic loading, are not suitable for mortar-less interlocking brick walls because the different response mode and sliding between mortar-less interlocking bricks greatly enhances the deformation capacity of the interlocking masonry wall.

4.3 Wall vibration frequency

White noise of small amplitude is applied to the wall after each ground excitation. Acceleration responses under white noise are analysed using stochastic subspace identification (SSI) and peak picking (PP) method to extract the horizontal in-plane natural frequency of the interlocking brick wall so as to quantify the damage severity of the interlocking brick wall after each test (Zhang 2007). As shown in Fig. 10, the natural frequency of the interlocking brick wall before the seismic excitation test is 12.29 Hz, which is slightly reduced to 12.2 Hz after subjected to PGA = 0.05 g and 0.1 g ground excitation, indicating no or little damage to the wall as observed visually in the test. After subjected to the 0.2 g loading, the frequency of the wall drops to 11.38 Hz, indicating minor damage to the wall. Under further increased ground excitations (0.3 g and 0.4 g), the frequency of the wall gradually reduces to 11.22 Hz and 10.54 Hz. It is to note that unlike conventional brick walls, whose damage develops quickly and natural frequency plummets in the face of earthquake loading (DeJong 2009), damage to the interlocking brick wall evolves relatively slowly. After subjected to the seismic excitation with a PGA of 0.5 g, the wall experiences substantial damage owing to the apparent rocking responses as described above, resulting in the reduction of natural frequency to 8.14 Hz. Considering the severe damage condition of the wall, no white noise excitation test is performed after the 0.6 g test.

4.4 Localised response mode

As described above, distinct local brick responses, i.e., brick rocking and sliding, are observed as the magnitude of the seismic loading increases. This local response could

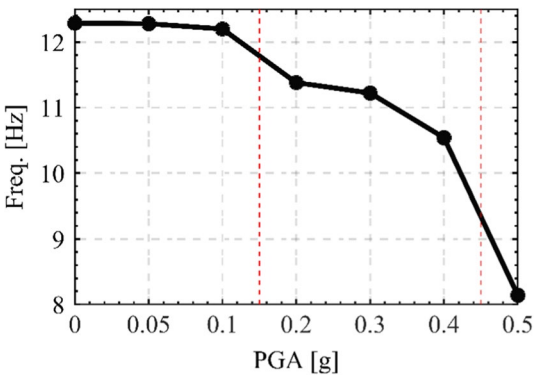

Fig. 10 In-plane natural frequency of the interlocking brick wall after seismic loadings of different PGAs

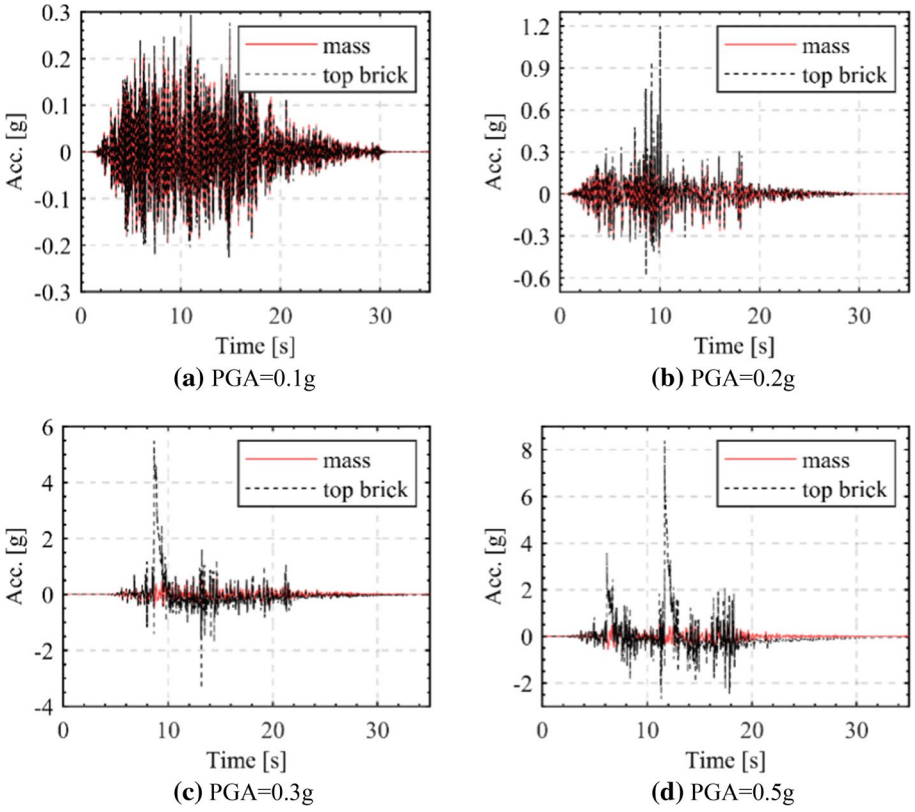

Fig. 11 Acceleration time history of the top brick and the mass

be discerned explicitly from the acceleration time history of the top brick and the added top mass. As shown in Fig. 11a, under 0.1 g loading when no local brick oscillation is visually observed, the acceleration time histories of the added mass and the top brick are almost identical because the added mass is firmly fixed to the brick wall. However, under the 0.2 g loading, an impulse is observed at around t = 10 s with an acceleration of over 1 g (Fig. 11b), owing to the occurrence of an inter-brick collision, which is a direct result of the localised movement of bricks. Similar spikes are also observed in the acceleration time histories in the subsequent tests with larger PGAs (Fig. 11c, d).

4.5 Energy dissipation mechanism

To further examine the seismic performance of interlocking brick wall, the energy dissipation mechanism is analysed. As described in Sect. 4.1, different from conventional mortar-bonded masonry walls, there is no distinct diagonal shear damage observed in the interlocking brick wall. Instead, rocking response of the wall is observed, as well as inter-brick sliding and pounding. The inter-brick pounding and friction both contribute to energy dissipation. The energy dissipation time histories of the scaled interlocking brick wall under the ground excitation are obtained through the validated numerical model. The energies dissipated by inter-brick friction and brick damage plus material

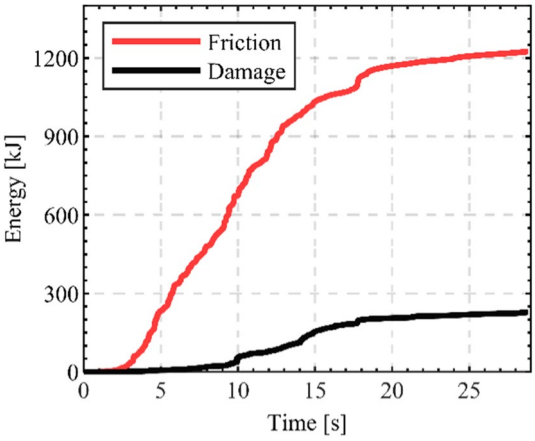

Fig. 12 Energy dissipated by different mechanisms in the 0.6 g excitation case

Table 5 Energy dissipated by different mechanisms

PGA (g)	Energy dissipated by friction (kJ)	Energy dissipated by brick damage and material plasticity (kJ)
0.2	34.58	0.00
0.3	74.99	0.06
0.4	173.82	0.28
0.5	510.82	18.73
0.6	1224.98	228.81

plasticity for the interlocking brick wall under 0.6 g ground excitation are shown in Fig. 12. It can be found that friction is the predominant energy dissipation mechanism, which gradually increases as the imposed seismic energy increases. The energy dissipated by the two mechanisms in other loading cases are tabulated in Table 5. As seen, energy dissipated by friction is remarkably larger than that by material plasticity and brick damage in all the cases with varying PGAs. It demonstrates that friction between the dry-stacking interlocking bricks contributes the most to the energy dissipation, while that consumed by brick damage and material plasticity is much smaller. Furthermore, very limited amount of energy is dissipated by material plasticity and brick damage before 0.5 g seismic loading, indicating minimum brick damages under these levels of excitations. Under these excitations, most seismic energy is consumed by friction between inter-brick sliding. This is an advantageous characteristic of interlocking brick wall with respect to the seismic resistance performance as compared to the conventional masonry walls.

5 Discussion on the seismic performance of interlocking brick walls

To further investigate the seismic performance of interlocking brick walls, numerical study is performed on full-scale masonry brick walls. Firstly, comparisons are made between an interlocking brick wall and a conventional CMU wall under seismic

excitations with varying PGAs to compare their seismic resistant capacity. Then, the influence of vertical components of seismic loading on the response of interlocking brick walls is investigated. It should be noted that usually vertical ground motion component is neglected in analysis and design of conventional masonry walls. However, vertical component may have a significant influence on interlocking brick wall owing to the observed rocking responses in the tests. The influence of velocity pulses of near-fault ground motions on the response of interlocking brick wall is also studied, which may also greatly affect the interlocking brick walls owing to the pounding responses between adjacent bricks.

5.1 Comparison between the interlocking brick wall and a CMU wall

5.1.1 Modelling of the full-scale walls

A conventional CMU wall is modelled with CMU blocks bonded by mortar, which replicates the most commonly constructed masonry structures. To validate the accuracy of the model, Turek et al.'s laboratory shaking table test on an unreinforced CMU wall (Turek 2002; Turek et al. 2007) is firstly numerically modelled for validation of the numerical model. This test is chosen to validate the model because significant diagonal shear-sliding response dominates the failure mode of the CMU wall, which can serve as a good reference to compare with the mortar-less interlocking brick wall. The wall in the test was 2400 mm (height) by 3000 mm (width) by 200 mm (thickness), constructed with 400 mm (width) by 200 mm (thickness) by 200 mm (height) concrete masonry blocks bonded by mortar. An added weight of 26.5 kN was applied on top of the wall. The shaking table test was conducted along the horizontal in-plane direction. The seismic record used in the shaking table test was generated from VERTEQII (Zone 4) response spectra defined in the standard GR-64-CORE (1995). A detailed three-dimensional numerical model of this CMU wall is generated in Abaqus, with CDP material model employed for the block material. The unconfined uniaxial compressive strength is 30 MPa following Turek et al.'s test. Type-S mortar with a compressive strength of 12 MPa was used to build the wall in the test (Turek 2002). As no other parameters of the mortar are provided, the cohesive parameters listed in Table 3, which belongs to a mortar with a compressive strength of 11.5 MPa, are adopted in this simulation for the cohesive contact between CMUs (Abdulla et al. 2017; Dassault Systèmes 2022). Figure 13a, b compare the damage initiation and final failure mode of the CMU wall in the test and those from the numerical simulation. According to Turek et al. (Turek 2002; Turek et al. 2007), the initial cracking in the tested wall was due to flexural components, showing mortar debonding as in Fig. 13a.) In the numerical simulation, similar mortar debonding is observed, as displayed in Fig. 13b. The final X-shape failure mode in the CMU wall as in the test is replicated by the numerical model, as seen in Fig. 13c, d. It should be noted that because the primary failure pattern before wall collapse changed from mortar debonding to serious shear-dominant failure, the damage state variable SDEG is hence adopted in Fig. 13d instead of contact slippage variable (CSLIP1, as used in Fig. 13b) to reflect the status of the wall. Since there are no quantitative results such as displacement time history available, only the observed damage mode is compared to verify the numerical model.

To compare the seismic response of the interlocking brick wall and the conventional CMU wall, two 2400 mm tall by 2400 mm wide load-bearing walls are numerically modelled. The aspect ratio (height-to-width) is set as 1.0 to be consistent with that in the

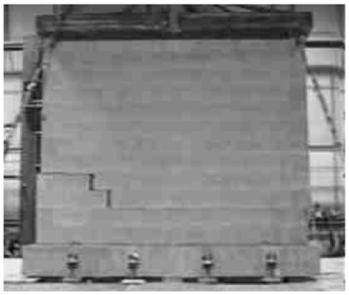

(a) Initial cracking (Turek 2002; Turek et al. 2007)

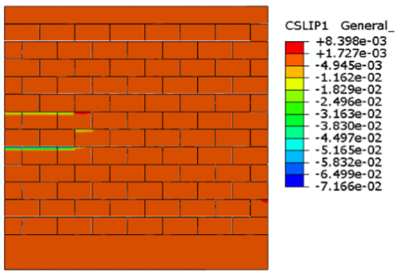

(b) Simulated initial inter-brick slippage (unit: mm)

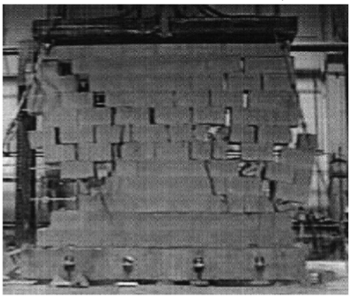

(c) Final wall failure mode (Turek 2002; Turek et al. 2007)

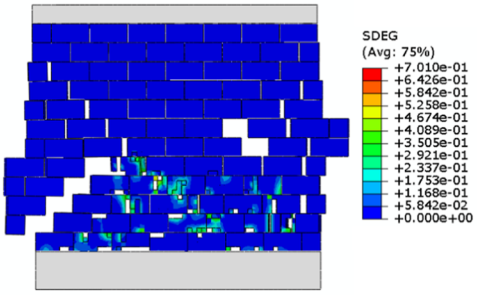

(d) Simulated final wall failure mode

Fig. 13 Comparison of CMU wall failure mode between the numerical simulation and the lab test results

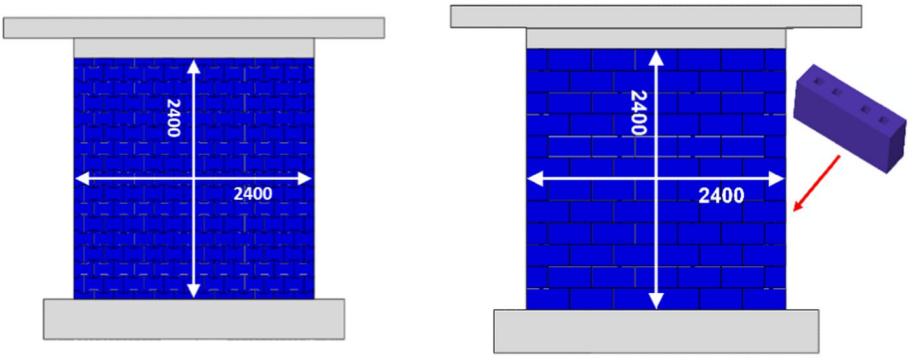

(a) Interlocking brick wall **(b)** Conventional CMU wall

Fig. 14 Full-scale models of the interlocking brick wall and the conventional CMU wall (unit: mm)

shaking table test (825/800 = 1.03) so that the failure mode of the full-scale interlocking brick wall under seismic loading would not be influenced by aspect ratio. The interlocking brick wall with the full-scale interlocking brick as illustrated in Fig. 2a is constructed using the dry-stacking (mortar-less) method (Fig. 14a), while the conventional brick wall is made of four-hole CMUs which have a unit thickness of 100 mm and a hole dimension of 30 mm × 30 mm and is bonded by mortar (Fig. 14b). Therefore, the cross-section area of

the interlocking brick wall is almost the same as that of the conventional CMU wall. The material parameters of the mortar follow those in reference (Abdulla et al. 2017), as listed in Table 3. For a fair comparison, the same brick material properties are considered in the numerical model for the CMUs and interlocking bricks using the CDP material model with an unconfined uniaxial compressive strength of 15 MPa and a Young's modulus of 19500 MPa, representing concrete of the same strength level (CCAA GUIDE HB 71 [T38] 2011). A mass block of 10.7t is set on the wall top to apply an axial load of 0.5 MPa. Four vertical reinforcing bars with a diameter of 12 mm are inserted at equal spacing in the voids of the bricks, providing a reinforcement ratio of 0.2%. Following prototype dimensions, the dimension of an interlocking brick is 200 mm (length) by 180 mm (height) by 100 mm (thickness). For the CMUs, the dimension of the block is 390 mm (length) by 190 mm (height) by 100 mm (thickness) bonded by a 10 mm-thick mortar layer (Concrete Masonry Association of Australia 2019). Cohesive contact with parameters listed in Table 3 is used to model the bonding behaviour between the CMU blocks. Such a modelling technique is commonly used for masonry structures (Abdulla et al. 2017). The seismic input used in the simulation is the one recorded at Station El Centro Array #9 in 1940 Imperial Valley-02 Earthquake (north–south direction) (University of California, Berkeley 2021). The amplitude is scaled to PGAs between 0.4 and 0.6 g. The acceleration time history with a scaled PGA of 0.5 g and the corresponding acceleration response spectra are shown in Fig. 15a, b, respectively.

5.2 Comparison of the seismic responses

Figure 16 shows the deformation and damage modes of the interlocking brick wall and the CMU wall under the ground excitations with varying intensities. As can be seen in Fig. 16a, when subjected to the seismic excitation with a PGA of 0.4 g, minor damage is observed on the two bottom corners of the interlocking brick wall as a result of the flexural response. By contrast, no damage occurs on the conventional CMU wall under the same level of seismic excitation (Fig. 16d). When subjected to PGA = 0.5 g seismic loading, the two bottom corners of the interlocking brick wall experience rocking induced damage, but the wall manages to survive the applied earthquake loading (Fig. 16b). In comparison, the

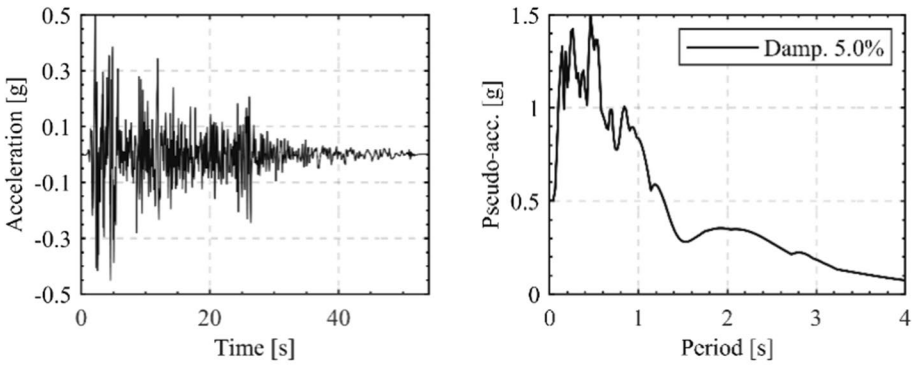

(a) Acceleration time history **(b)** Acceleration response spectra

Fig. 15 The seismic excitation of the 1940 Imperial Valley-02 Earthquake (Station El Centro Array#9, north–south direction, PGA = 0.5 g)

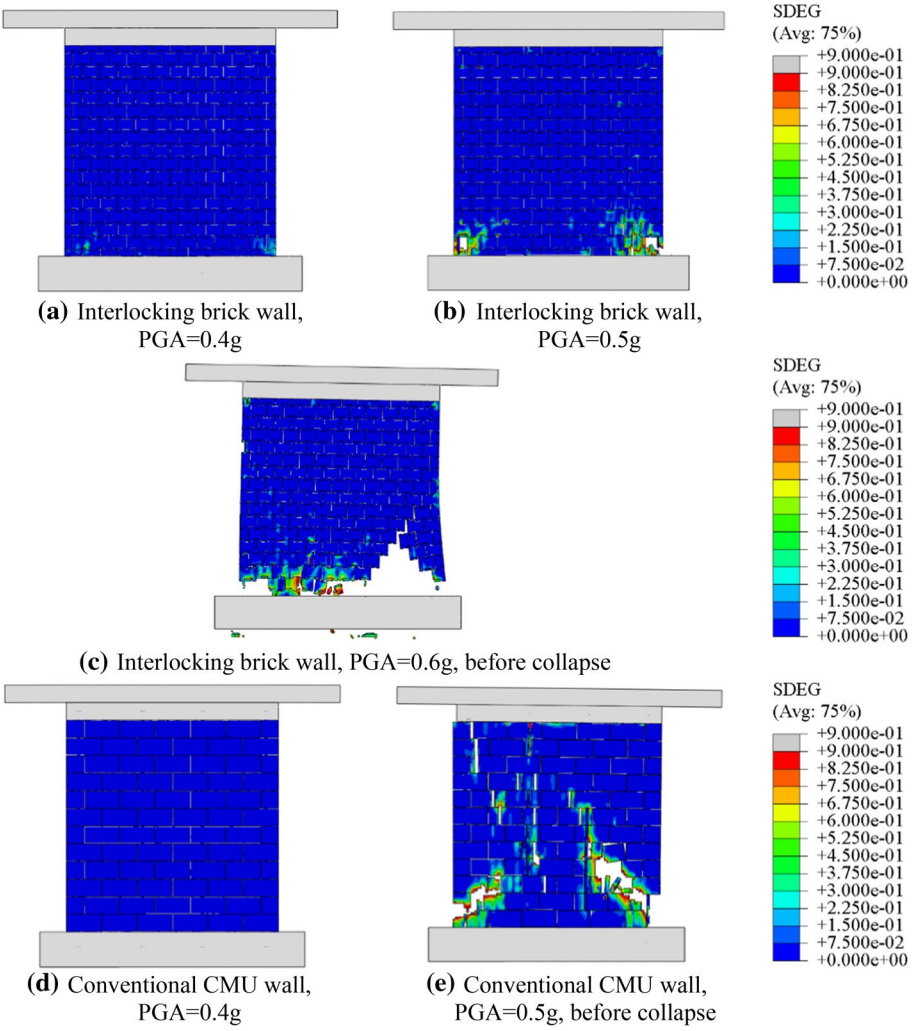

Fig. 16 Deformation and damage modes of the walls under seismic excitation with varying intensities (PGA)

conventional CMU wall experiences severe toe crushing under the seismic loading with a PGA of 0.5 g. The damage then develops diagonally upwards and eventually causes collapse of the wall (Fig. 16e). Numerical modelling on the interlocking brick wall is extended with a larger PGA (0.6 g). As can be seen in Fig. 16c, under PGA = 0.6 g ground excitation, damage initiates at the two bottom corners; rocking further leads to the crushing failure of the bricks. The damage then extends inward and eventually results in the total collapse of the interlocking brick wall under flexural failure. It is worth noticing that no diagonal shear cracking is observed.

As shown in Fig. 17a–c, the hysteresis curves of the interlocking brick walls exhibit a pinching character, especially under 0.5 g and 0.6 g loading, indicating the interlocking brick walls are dominated by flexural response under seismic excitation (Magenes and

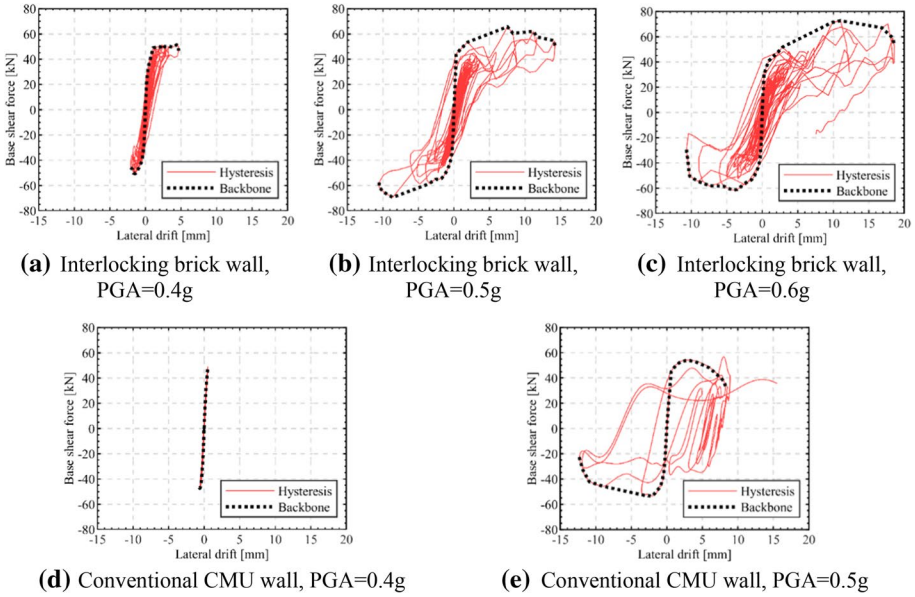

(a) Interlocking brick wall, PGA=0.4g **(b)** Interlocking brick wall, PGA=0.5g **(c)** Interlocking brick wall, PGA=0.6g

(d) Conventional CMU wall, PGA=0.4g **(e)** Conventional CMU wall, PGA=0.5g

Fig. 17 Hysteretic curves and backbone curves of the walls subjected to seismic excitations of varying PGAs

Calvi 1997). This is because the interlocking brick wall has a relatively high shear resistance provided by the interlocking keys compared to the mortar bonding of CMU walls. Figure 17a displays the hysteresis curve of the interlocking brick wall under the seismic excitation with a PGA of 0.4 g. An initial stiffness of 140.7 kN/mm is obtained from the linear part of the backbone curve. Under PGA = 0.5 g seismic excitation (Fig. 17b), the initial stiffness is 139.7 kN/mm, which quickly deteriorates to 30.5 kN/mm after the wall experiences nonlinear response. The peak base shear force is 69.5 kN, while the ultimate drift is 14.2 mm. When the interlocking wall is subjected to 0.6 g ground excitation (Fig. 17c), the wall shows a similar initial stiffness (131.0 kN/mm), which degrades to 18.6 kN/mm, denoting a more significant wall damage. It should be noted that the observed slightly smaller initial stiffness of the same wall model under gradually increased ground excitations indicates a larger ground excitation induces more local sliding and brick rocking response, which slightly reduces the stiffness of the interlocking masonry wall. Because of the larger ground excitation, the peak base shear force (72.6 kN) and the ultimate lateral drift (18.6 mm) are also larger.

Figure 17d shows the hysteresis curve and the backbone curve of the conventional CMU wall subjected to the seismic excitation with a PGA of 0.4 g. The conventional CMU wall shows almost linear behaviour under this seismic excitation level, with a stiffness of 81.7 kN/mm, which is much lower than that of the interlocking brick wall. The hysteresis curve of the conventional CMU wall subjected to the seismic excitation with a PGA of 0.5 g is plumper compared to those of the interlocking brick walls, as shown in Fig. 17e, signifying a shear-dominant brittle damage response mode (Magenes and Calvi 1997). The initial stiffness of the conventional CMU wall is 80.7kN/mm. The peak base shear force and the ultimate lateral drift before wall collapse are 54.04 kN and 12.3 mm, respectively, both are much lower than those of the interlocking brick wall, indicating the seismic

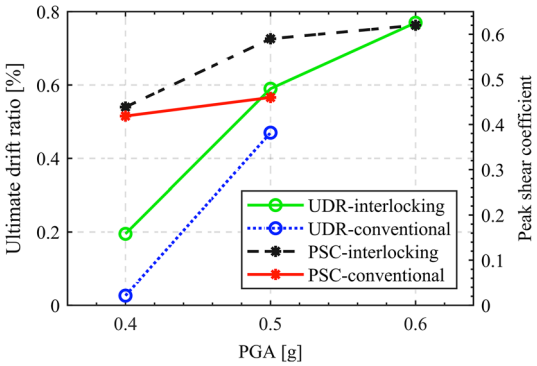

Fig. 18 Ultimate drift ratios and peak shear coefficients under seismic excitation with varying intensities

resistance capacity and the deformability of the conventional CMU wall are lower than those of the interlocking brick wall.

The peak shear coefficient and the maximum drift ratio are summarised in Fig. 18. The shear coefficient, *C*, is defined as the ratio of base shear force to total weight of the wall (Benedetti et al. 1998; Kallioras et al. 2018), where both the interlocking brick wall and the CMU wall have the same total weight of 11.94t. As can be seen, for the interlocking brick wall, the peak shear coefficient is 0.44 under the PGA = 0.4 g seismic excitation, which increases significantly to 0.59 when the PGA increases to 0.5 g, and then increases by a small amount to 0.62 when the PGA increases to 0.6 g. The slight difference of the peak shear coefficients in the latter two cases reveals that under increased seismic loadings, the shear strength of the interlocking brick wall is not the dominant parameter. Instead, the failure of the interlocking brick wall is dominated by flexural bending failure. In comparison, the peak shear coefficient for the conventional CMU wall is 0.42 under PGA = 0.4 g seismic excitation and 0.46 under PGA = 0.5 g seismic excitation. Comparing the conventional CMU wall with the interlocking brick wall under PGA = 0.5 g seismic loading, both the walls show apparent nonlinear behaviour. The peak shear coefficient of the interlocking brick wall is about 20% higher than that of the conventional CMU wall, which demonstrates that the interlocking brick wall has a better seismic resistance capacity. On the other hand, under PGA = 0.5 g seismic excitation, the ultimate drift ratio of the CMU wall is 0.47% and the wall collapses. In comparison, the ultimate drift ratios of the interlocking brick wall under PGA = 0.5 g and 0.6 g seismic loading are 0.59% and 0.77%, respectively. Therefore, the interlocking brick wall has a higher lateral deformation capability than the conventional CMU wall under seismic loading.

As demonstrated in Sect. 4.5, for interlocking brick walls, significant amount of energy is consumed by inter-brick friction in lieu of brick material damage. To validate this finding, the ratios of energy dissipated by friction to that by material damage under different seismic intensities for the interlocking brick wall and the conventional CMU wall are summarised in Fig. 19. It is apparent that inter-brick friction serves as the dominant energy dissipation source for interlocking brick walls in all the modelled loading cases. The ratio of friction-dissipated energy to brick-material-damage-consumed energy quickly reduces as the imposed ground excitation intensity increases. When subjected to the PGA = 0.4 g seismic loading, the ratio for the interlocking brick wall is as high as 42.36. As the seismic input intensity increases, the ratio gradually decreases to 7.25 and 5.59 for the PGA = 0.5 g and PGA = 0.6 g cases, respectively, implying increased damage to bricks. In comparison,

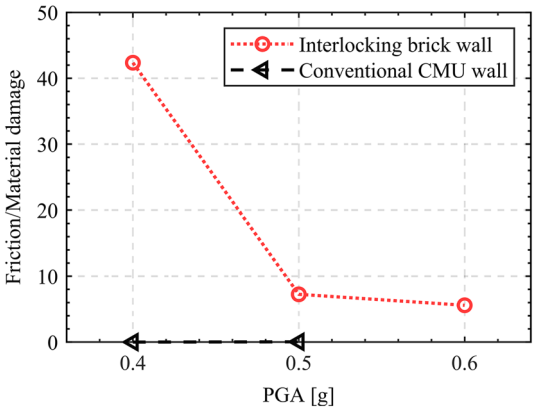

Fig. 19 Ratios of energy dissipated by friction and material damage under varying seismic intensities

for the CMU wall, little energy is dissipated by inter-brick friction. This is because mortar bonding leads to very rigid and brittle nature of conventional CMU wall.

5.3 The influence of vertical components of seismic loading

In the tests, rocking response is observed as a predominant mode governing the failure of interlocking brick walls under seismic loading. Since the vertical component of a seismic loading, which is normally ignored in analysis and design of masonry walls, would affect the behaviour of the interlocking brick wall, influences of vertical component of seismic ground motion on interlocking brick wall need be investigated. To examine this influence, numerical modelling is performed on an interlocking brick wall subjected to horizontal only in-plane ground excitation, and both the horizontal and vertical excitations. The recorded horizontal and vertical ground excitations at Station HWA032 in the 1999 Chi-Chi Earthquake (University of California, Berkeley 2021) is employed. The horizontal component is scaled to a PGA of 0.6 g, and the corresponding vertical component is scaled by the same factor as used in the horizontal direction, yielding a PGA of 0.35 g. Figure 20a, c show the scaled horizontal and vertical seismic ground motion, respectively, with their pseudo-acceleration response spectra shown in Fig. 20b, d. The interlocking brick wall is 2400 mm wide, 2400 mm high and 100 mm thick. The axial load, reinforcement ratio and brick material properties are the same as in Sect. 5.1.2, i.e., a 0.5 MPa axial load (provided by a top mass of 10.7t), a reinforcement ratio of 0.2% (provided by four 12 mm-diameter un-pretensioned reinforcement bars), and brick material with a compressive strength of 15 MPa and a Young's modulus of 19500 MPa.

Figure 21 illustrates the damage contours of the two walls. It can be found that with horizontal excitation only, the two bottom corners of the interlocking brick wall experience damages due to rocking response (Fig. 21a). The damage at the two corners is increased substantially when the vertical component of the seismic loading is also considered (Fig. 21b), owing to more substantial rocking response. This comparison demonstrates that the vertical excitation amplifies the response and damage of the interlocking brick wall. The result indicates that the interlocking brick walls need be properly anchored to mitigate rocking responses. This, however, is beyond the scope of the current paper, and will be a study topic in the near future.

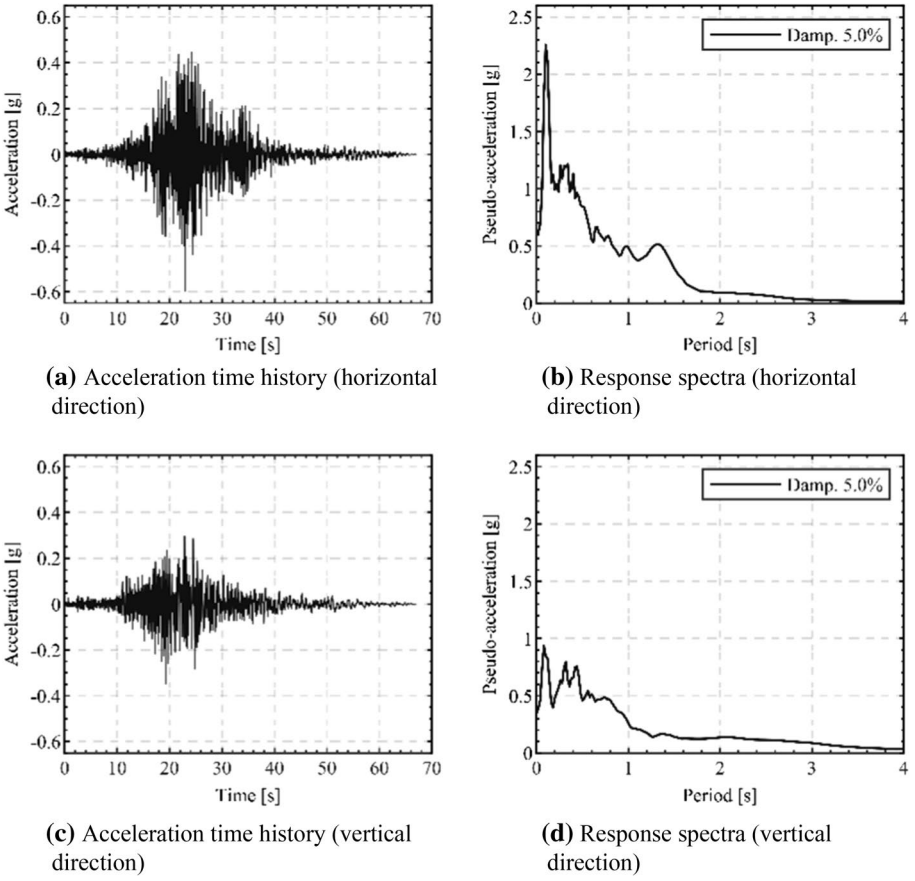

(a) Acceleration time history (horizontal direction)

(b) Response spectra (horizontal direction)

(c) Acceleration time history (vertical direction)

(d) Response spectra (vertical direction)

Fig. 20 The seismic excitation of 1999 Chi-Chi Earthquake (Station HWA032) used in this study

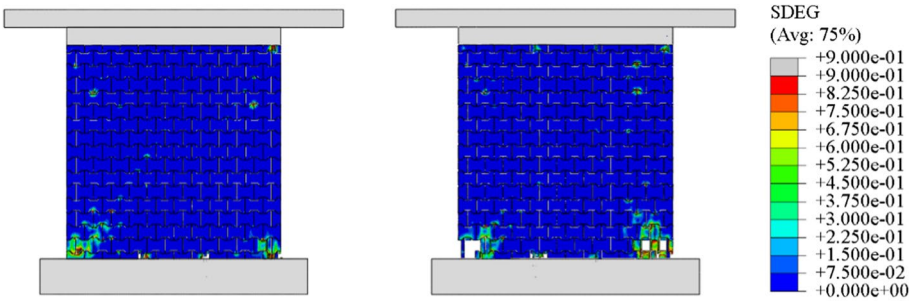

(a) Horizontal excitation only

(b) Horizontal and vertical excitations

Fig. 21 Damage of the interlocking brick walls under seismic excitations with or without considering the vertical ground excitation

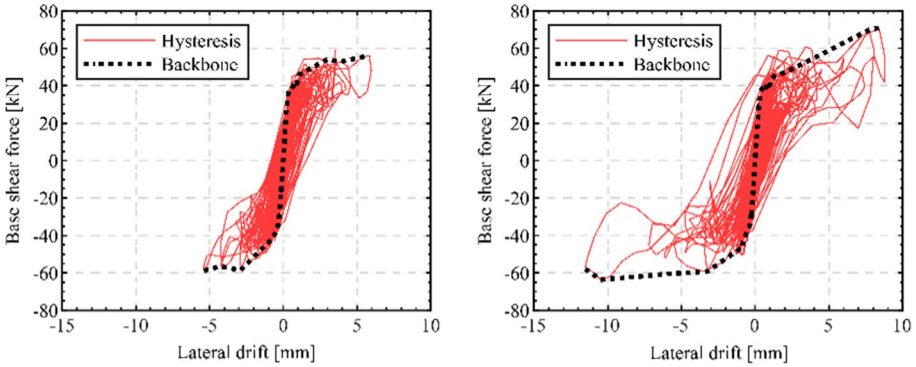

Fig. 22 Hysteresis curves and backbone curves of the interlocking brick walls under seismic excitations with or without vertical components

The hysteresis curves and the backbone curves of the interlocking brick walls subjected to the horizontal and simultaneous horizontal and vertical ground motions are sketched in Fig. 22. As shown in Fig. 22a, the maximum drift of the wall subjected to only the horizontal excitation is 6 mm, namely a drift ratio of 0.25%, denoting a minor damage level of the wall. In contrast, when the vertical component of the seismic loading is considered, the hysteretic curve in Fig. 22b shows a pronounced asymmetry with the negative drift significantly larger than the positive one, reaching a value of 11.5 mm, which corresponds to a maximum drift ratio of 0.48%. The significant increase in the wall peak drift ratio is the consequence of severe damage to the left toe of the wall, resulting from a more substantial rocking response. It should be noted that in the tests, only horizontal excitation is applied, and the wall does not collapse when the drift ratio is 3.4% as presented in Sect. 4.2. However, when both horizontal and vertical ground motions are considered simultaneously, large damage to the wall is observed when the draft ratio is 0.48% only. This is because rocking responses are the primary source causing damage to the toe of the interlocking brick wall, while vertical motion enhances rocking response of the wall, which leads to the tensile failure and falling off of the interlocking bricks at the corners of the wall. These

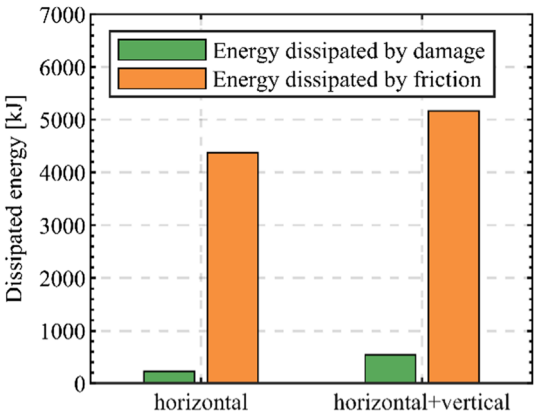

Fig. 23 Comparison of energy dissipations of the interlocking brick walls under seismic excitations with or without vertical components

results indicate that vertical ground excitation cannot be neglected in analysing the seismic responses of interlocking brick walls. Increasing the confinement between interlocking bricks, especially in the toe areas of the wall and providing anchors to mitigate rocking responses would increase the seismic resistance capacity of the interlocking brick walls. Further study to quantitatively investigate this will be carried out in the near future.

Figure 23 compares the energy dissipated by inter-brick friction and material damage, respectively. It can be found that the inter-brick friction consumed slightly more energy from 4377 to 5161 kJ (an increase of 17.9%) when the vertical component of the seismic loading is considered, indicating the inter-brick sliding and oscillation is not greatly influenced. However, the energy dissipated by material damage increases from 225 to 541 kJ, an increase of 140.4%. This is due to the more severe brick damage resulting from more pronounced rocking response when the vertical component of the seismic loading is included. It is worth noting that despite the aggravated damage, friction is still the predominant energy dissipation mechanism.

5.4 The influence of ground motion pulses

Pulse-like seismic excitations could induce more severe damage to structures than non-pulse-like loading of the same magnitude because of a higher energy input velocity (Bertero et al. 1978; Housner and Hudson 1958; Pan et al. 2017; Zhang et al. 2020), which may have a more detrimental effect on interlocking brick walls as impacting between adjacent bricks were observed in the tests. To investigate the potential influence of pulse-like seismic excitation on the interlocking brick wall response, two numerical simulations are performed on an interlocking brick wall subjected to a pulse-like seismic record and a non-pulse-like one, respectively. The interlocking brick wall considered in the analysis is the same as the one in Sect. 5.2. Both seismic waves are recorded during the 1999 Chi-Chi Earthquake (University of California, Berkeley 2021). The pulse-like wave is recorded from Station CHY101, while the non-pulse-like record is from Station HWA032. Figure 24 shows the acceleration and velocity time histories (Fig. 24a–d) and the corresponding response spectra (Fig. 24e–h) of the two records (both scaled to 0.6 g).

Figure 25 illustrates the damage contours of the two interlocking brick walls under the pulse-like (Fig. 25a) and non-pulse-like (Fig. 25b) ground excitations. Toe damages can be observed in both walls as a result of the rocking response. No distinctive difference could be observed between their damage distribution. The hysteresis curves of the two walls are displayed in Fig. 26. The pulse-like loading (CHY101) induces a larger drift and a higher base shear force than the non-pulse-like excitation. Under the pulse-like excitation (Fig. 26a), the peak base shear force is 73.1 kN, and the maximum drift is 10.7 mm (a drift ratio of 0.45%). In comparison, under the non-pulse like seismic excitation (Fig. 26b), the peak base shear force is 58.6 kN and the maximum drift is 6 mm (corresponding to a drift ratio of 0.25%). A more distinctive pinching shape is also observed in the hysteresis curve of the wall subjected to the pulse-like excitation. The above comparisons demonstrate that the interlocking brick wall experiences a higher extent of flexural response when subjected to the pulse-like ground excitation (CHY101) than that subjected to the non-pulse-like excitation (HWA032). However, the velocity pulse has no pronounced effect on the wall responses, as will be further examined below. The difference of the peak shear force and maximum lateral drift of the wall under the two seismic excitations are attributed to the differences in the two ground excitations, e.g., the differences in frequency contents.

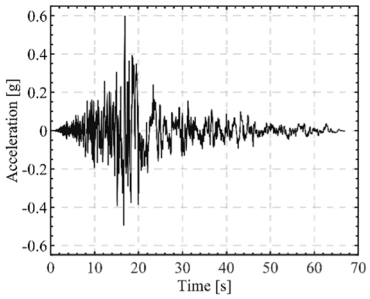

(a) CHY acceleration time histories

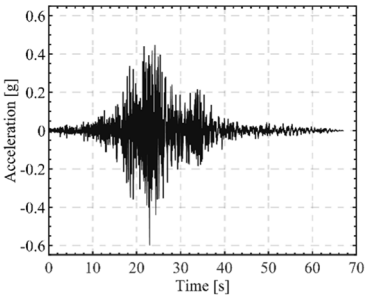

(b) HWA acceleration time histories

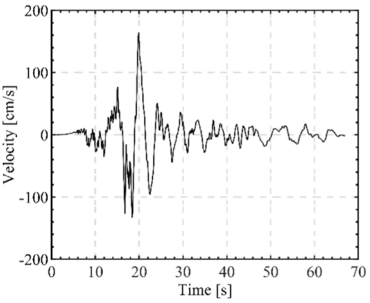

(c) CHY velocity time histories

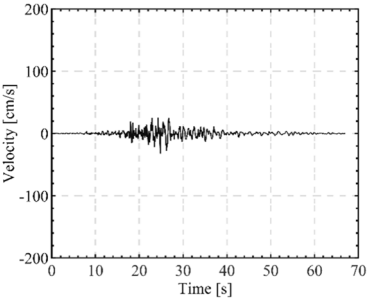

(d) HWA velocity time histories

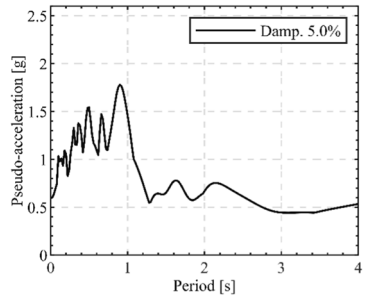

(e) CHY acceleration response spectra

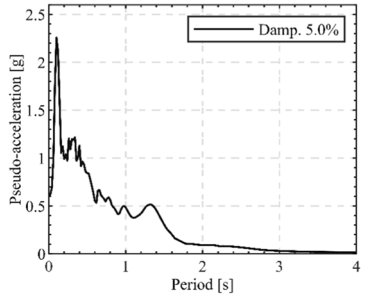

(f) HWA acceleration response spectra

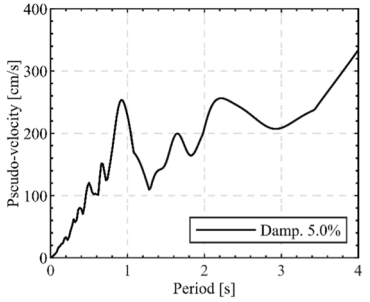

(g) CHY velocity response spectra

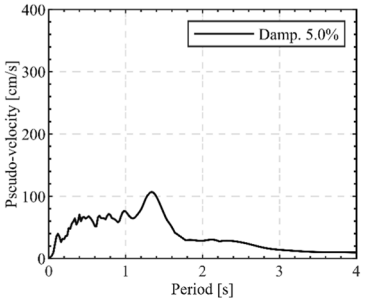

(h) HWA velocity response spectra

Fig. 24 Acceleration time histories, velocity time histories, acceleration response spectra and velocity response spectra of the chosen seismic records

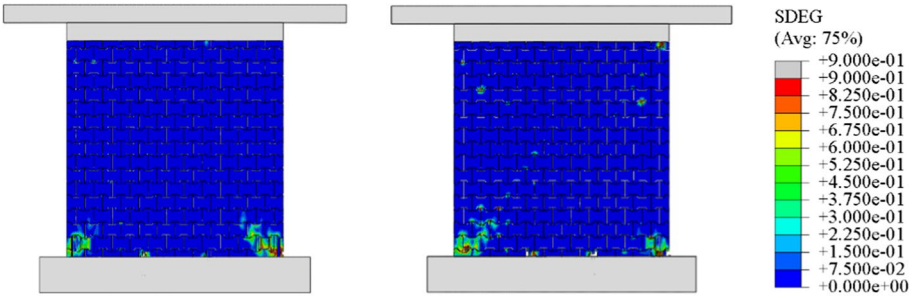

(a) CHY (pulse-like) **(b)** HWA (non-pulse-like)

Fig. 25 Damage mode of the interlocking brick wall under pulse-like and non-pulse-like seismic excitations

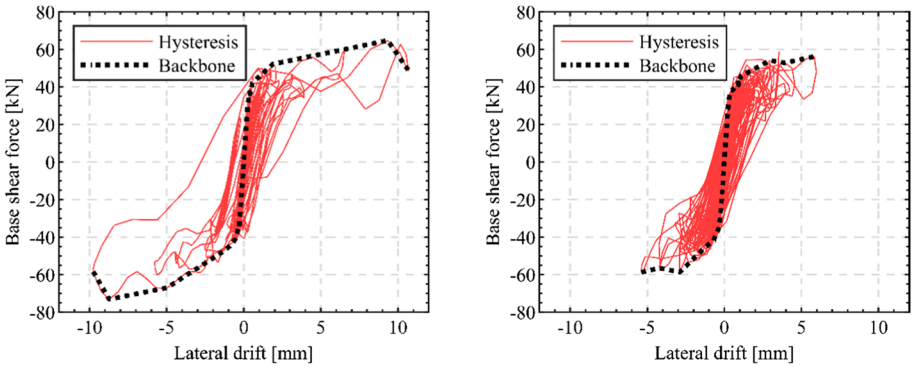

(a) CHY (pulse-like) **(b)** HWA (non-pulse-like)

Fig. 26 Hysteresis curves and backbone curves of the interlocking brick walls under pulse-like and non-pulse-like seismic excitations

To examine the influence of the ground velocity pulse on the seismic response of the interlocking brick wall, the input pulse-like excitation and the output in-plane horizontal velocity time history at the top of the wall are extracted using Baker et al.'s method (Baker 2007; Baker and Cornell 2008; Shahi and Baker 2014, 2019). The fourth-order Daubechies wavelet is chosen as the mother wavelet because it matches well with many velocity pulses observed in near-fault ground motions (Baker 2007). As shown in Fig. 27a, the velocity time history of the input ground excitation and the velocity response of the interlocking brick wall match closely with each other. The input velocity pulse occurs at around 20 s, with a peak value of 143.2 cm/s (Fig. 27b). The interlocking brick wall is observed to have an identical velocity pulse, with almost the same peak value (142.2 cm/s) at the same time instant (Fig. 27b), indicating that the velocity pulse of the ground motion excites a rigid-body movement of the interlocking brick wall without significant deformation. Differences can only be observed in the residual part of the velocity time histories between the input ground motion and the output interlocking brick wall response. As seen in Fig. 27c, a peak ground motion velocity of 39.89 cm/s occurs at t = 17.02 s, while a peak velocity response is 57.66 cm/s at t = 17.07 s (a difference of 44.5%). Such observation indicates that the interlocking brick wall is not susceptible to the velocity pulses of ground motion. On the

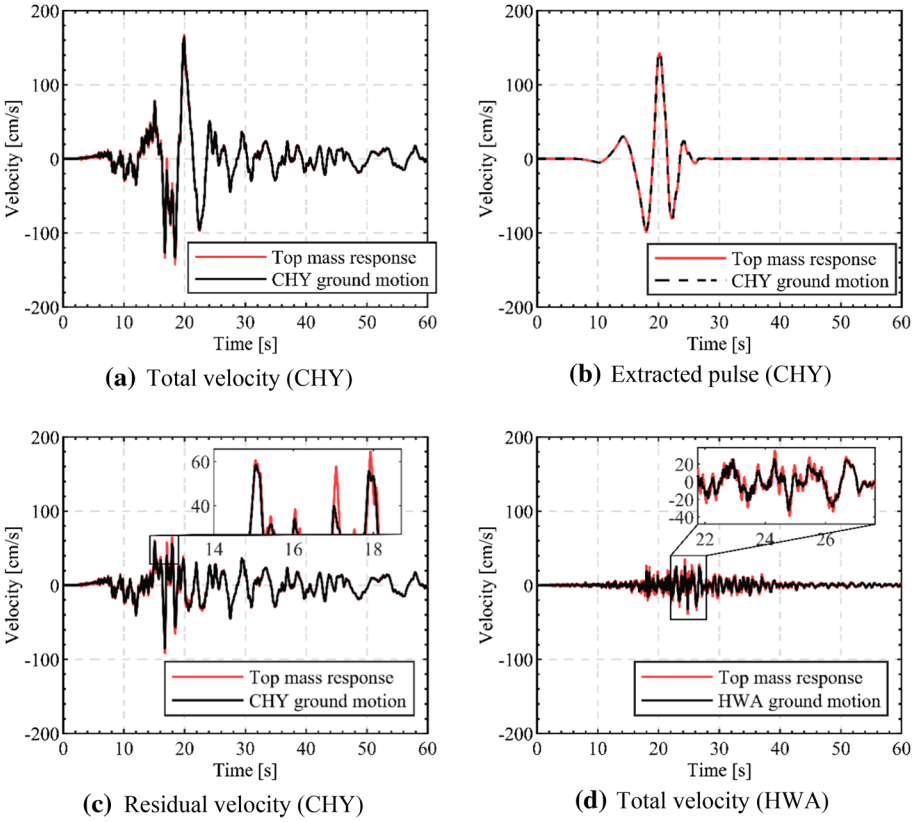

Fig. 27 Velocity pulse extraction of the CHY ground motion and of the response of the top mass of the interlocking brick wall

other hand, the HWA ground excitation is a typical far-fault ground motion. No velocity pulse components are involved in its velocity time history. Hence, no velocity pulses can be extracted from the velocity response of the interlocking brick wall. Comparison of the velocity response of the top mass and the input velocity of the HWA ground motion (the non-pulse-like one) is shown in Fig. 27d, where slight differences are observed between the ground motion velocity and the response velocity, similar to what is seen in Fig. 27c, demonstrating again the interlocking brick wall is not sensitive to ground motion velocity pulses.

The above comparison shows that the interlocking brick wall is insensitive to velocity pulse. This is because of the relatively high natural frequency of the interlocking brick wall resulting from its large lateral stiffness provided by the interlocking keys. Using the Lanczos algorithm (Dassault Systèmes 2022), the fundamental frequency of the interlocking brick wall (in the in-plane direction) is found to be 18.29 Hz. As pointed out in references (Chopra 2014; Chopra and Chintanapakdee 2001; Malhotra 1999), a system with a high fundamental frequency is more sensitive to acceleration input but less sensitive to input velocity and displacement under a pulse-like ground motion as its behaviour resembles a rigid body which moves together with the ground. Moreover, the dominant frequency of the velocity pulse shown in Fig. 27b is only 0.18 Hz. Such a low dominant frequency is a

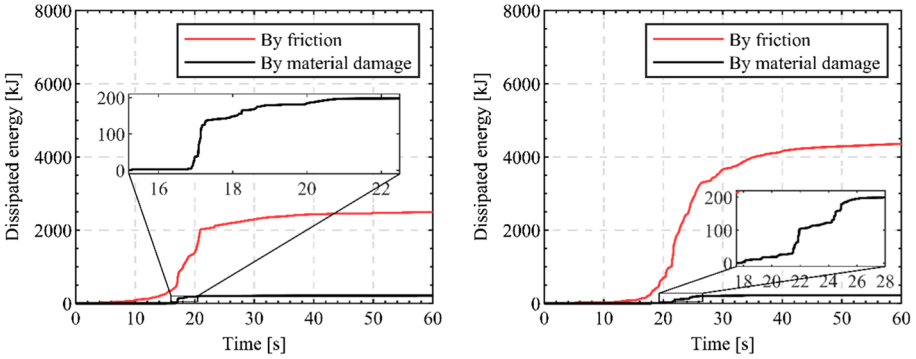

(a) Interlocking brick wall subjected to CHY excitation

(b) Interlocking brick wall subjected to HWA excitation

Fig. 28 Energy dissipated by different mechanisms under pulse-like and non-pulse-like ground motions

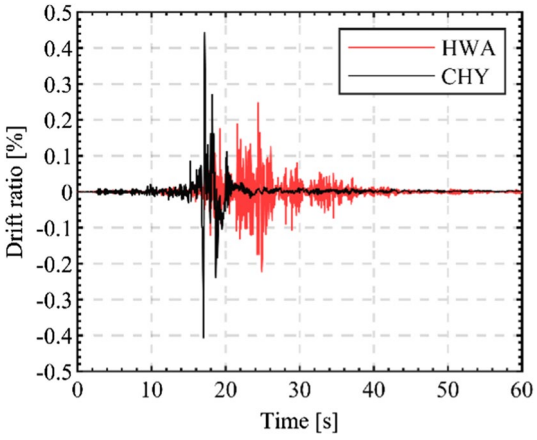

Fig. 29 Drift ratio time histories of the interlocking brick wall under pulse-like and non-pulse-like ground motions

common feature of the velocity pulse of near-fault ground motions (Somerville and Graves 1993). Hence, the frequency of the ground pulse is much smaller and far different from the vibration frequency of the interlocking brick wall. As a result, velocity pulse does not impose much influence on the response of the interlocking brick wall.

To further elucidate the above findings, the energies dissipated by brick material damage and inter-brick friction under the pulse-like and non-pulse like ground motions are derived and shown in Fig. 28a, b, respectively, while the comparison between the drift ratio time histories of the wall under the two ground motions is displayed in Fig. 29. When the interlocking brick wall is subjected to the pulse-like ground excitation, brick damage induced energy dissipation suddenly rises at around t = 17 s due to the peak acceleration of the CHY ground motion; the peak drift ratio (0.45%) of the wall also occurs at this time. Afterwards at t = 20 s, when the velocity pulse comes, there is barely change in the energy dissipation time histories associated to brick damage; likewise, only a small spike of the drift ratio time history curve is observed around this time. This proves that the velocity pulse does not boost the damage of the interlocking brick wall. On the other hand, the

inter-brick friction dissipated energy accumulates during t = 4–21 s, associated with the relatively large acceleration inputs. This demonstrates that the interlocking brick wall is more sensitive to ground acceleration than to velocity. In comparison, when the same interlocking brick wall is subjected to the non-pulse like HWA ground excitation, energy dissipated by inter-brick friction is accumulated over a much longer duration from t = 12–41 s, throughout the majority of the ground excitation process.

Overall, the energy dissipated by inter-brick friction is still more pronounced over that by brick material damage. When subjected to the two different ground excitations, brick material damage induced energy dissipation is very similar, namely 214 kJ under CHY ground excitation (pulse-like), and 225 kJ under HWA ground excitation (non-pulse like). This demonstrates that similar levels of brick damage are induced in the interlocking brick wall under the two seismic excitations. However, when subjected to the non-pulse-like ground excitation, a total of 4377 kJ energy is dissipated by friction, which is significantly larger than that under the pulse-like ground excitation (2493 kJ). This is because the input energy of the pulse-like CHY ground motion concentrates around the velocity pulse at around t = 20 s (Housner and Hudson 1958), while the input energy of the non-pulse-like HWA ground motion distributes in a relatively long duration. Using Uang et al. and Ohi et al.'s method to calculate the energy input by ground motion (Ohi et al. 1991; Uang and Bertero 1990), the inputted energy to the interlocking brick wall by the pulse-like CHY ground motion is 3745 kJ, while it is 7111 kJ by the non-pulse like HWA ground motion. The above results further prove that the interlocking brick wall is not sensitive to velocity pulses of near-fault ground motions. Instead, the interlocking brick wall is more sensitive to ground accelerations, which are more likely to excite local brick oscillation and inter-brick friction.

6 Conclusions

In this study, laboratory shaking table tests and numerical modelling are performed to investigate the seismic performance of mortar-less interlocking brick wall. Laboratory shaking table tests are firstly carried out on a scaled interlocking brick wall. Then, a detailed numerical model is generated and validated with the laboratory testing results. A series of numerical simulations are subsequently carried out to compare the seismic resistance capacity of the interlocking brick wall and the conventional masonry wall. The influences of vertical components of a seismic excitation, and the velocity pulse contained in near-fault ground motion on the seismic behaviour of the interlocking brick wall are studied in the aspects of damage modes, drift ratios, peak shear coefficients and energy dissipation mechanisms. The following conclusions are drawn from this study:

1. Under seismic loading, the interlocking brick wall tends to develop rocking response leading to toe crushing.
2. Apparent inter-brick oscillation is observed in the interlocking brick walls, leading to a substantial amount of energy dissipation through friction, which greatly outweighs the energy dissipated by brick damage.
3. Because of the shear keys, which increases the shear capacity of the wall, the response and damage of interlocking brick wall are governed by rocking response associate with the flexural bending of the wall; the interlocking brick wall exhibits a higher seismic

resistance than the conventional CMU wall in terms of the strength and deformation capacity when subjected to horizontal seismic excitations. However, interlocking brick wall is susceptible to vertical ground excitation, therefore vertical ground excitation should not be neglected in the analysis and design of interlocking brick walls. This susceptibility may be solved by introduction of interlocking mechanism in vertical direction and properly anchoring the wall on the footings, which will be further assessed in future study as part of the optimisation of interlocking shapes and interlocking brick wall design.

4. The interlocking brick wall is found insensitive to velocity pulses in near-fault ground motions, but sensitive to ground acceleration due to its relatively high in-plane natural frequency.

Acknowledgements The first three authors would like to acknowledge the financial support from Australian Research Council (ARC) under the ARC Linkage Project LP170100846 for conducting this study. The authors also appreciate the Pacific Earthquake Engineering Research Centre (PEER) for the seismic record data.

Author contributions GX conducted the laboratory test and numerical simulation, analysed the data, and drafted the manuscript. XZ guided the laboratory test and numerical simulation, revised the manuscript in detail, and agrees to be accountable for all aspects of the work in ensuring that questions related to the accuracy or integrity of any part of the work are appropriately investigated and resolved. HH initiated the project, defined the research scope and direction, revised the manuscript critically for important intellectual content, provided explanations and interpretations of the observed results from experimental tests and numerical simulations of the interlocking brick wall under seismic excitations, and approved the version for publication. KB generated the synthetic seismic record used in the laboratory shaking table test and helped revise the manuscript. YL gave suggestions in processing the recorded structural response and extracting the velocity pulses from the input ground motion and the output structural response in numerical simulation. All authors read and approved the final manuscript.

Funding Open Access funding enabled and organized by CAUL and its Member Institutions. This research was supported by Australian Research Council (ARC) under the ARC Linkage Project LP170100846.

Data availability The data that support the findings of this study are available from the corresponding author upon reasonable request.

Code availability Not applicable.

Declarations

Conflict of interest The authors declare that they have no conflict of interest.

Consent to participate All the authors have read the final manuscript and agreed to be authors of it.

Consent for publication All the authors have read and agreed to submit the paper to Bulletin of Earthquake Engineering (BEE).

References

(2011) CCAA GUIDE HB 71 [T38]: reinforced concrete design handbook in accordance with AS3600–2009, 5th edn. CCAA Technical Publications - All Series. Cement Concrete & Aggregates Australia (CCAA), Sydney, NSW

Abdulla KF, Cunningham LS, Gillie M (2017) Simulating masonry wall behaviour using a simplified micro-model approach. Eng Struct 151:349–365. https://doi.org/10.1016/j.engstruct.2017.08.021

Ahmed A, Afreen A, Moin K (2017) State of art review: behaviour of masonry structures under gravity and seismic loads. Int J Emerg Technol Adv Eng 7:202–214

Al-Fakih A, Mohammed BS, Nuruddin F, Nikbakht E (2018) Development of interlocking masonry bricks and its' structural behaviour: a review paper. IOP Conf Ser Earth Environ Sci 140:1–9. https://doi.org/10.1088/1755-1315/140/1/012127

Ali M, Chouw N (2013) Experimental investigations on coconut-fibre rope tensile strength and pullout from coconut fibre reinforced concrete. Constr Build Mater 41:681–690. https://doi.org/10.1016/j.conbuildmat.2012.12.052

Ali M, Gultom RJ, Chouw N (2012) Capacity of innovative interlocking blocks under monotonic loading. Constr Build Mater 37:812–821. https://doi.org/10.1016/j.conbuildmat.2012.08.002

Ali M, Briet R, Chouw N (2013) Dynamic response of mortar-free interlocking structures. Constr Build Mater 42:168–189. https://doi.org/10.1016/j.conbuildmat.2013.01.010

Anand KB, Ramamurthy K (2000) Development and Performance evaluation of interlocking-block masonry. J Archit Eng 6:45–51. https://doi.org/10.1061/(ASCE)1076-0431(2000)6:2(45)

Anand KB, Ramamurthy K (2005) Development and evaluation of hollow concrete interlocking block masonry system. Masonry Soc J 23:11–19

Aslam M, Godden WG, Scalise DT (1980) Earthquake rocking response of rigid bodies. J Struct Div 106:377–392. https://doi.org/10.1061/JSDEAG.0005363

Baker JW (2007) Quantitative classification of near-fault ground motions using wavelet analysis. Bull Seismol Soc Am 97:1486–1501. https://doi.org/10.1785/0120060255

Baker JW, Cornell CA (2008) Vector-valued intensity measures for pulse-like near-fault ground motions. Eng Struct 30:1048–1057. https://doi.org/10.1016/j.engstruct.2007.07.009

Benedetti D, Carydis P, Pezzoli P (1998) Shaking table tests on 24 simple masonry buildings. Earthq Eng Struct Dyn 27:67–90. https://doi.org/10.1002/(SICI)1096-9845(199801)27:1%3c67:AID-EQE719%3e3.0.CO;2-K

Bertero VV, Mahin SA, Herrera RA (1978) Aseismic design implications of near-fault San Fernando earthquake records. Earthq Eng Struct Dyn 6:31–42. https://doi.org/10.1002/eqe.4290060105

Bhartiya R, Sahoo DR, Verma A (2021) Modified damaged plasticity and variable confinement modelling of rectangular CFT columns. J Constr Steel Res 176:106426. https://doi.org/10.1016/j.jcsr.2020.106426

Bi K, Hao H (2012) Modelling and simulation of spatially varying earthquake ground motions at sites with varying conditions. Probab Eng Mech 29:92–104. https://doi.org/10.1016/j.probengmech.2011.09.002

Bland DW (2011) In-plane cyclic shear performance of interlocking compressed earth block walls

Bosro MZM, Samad AAA, Mohamad N, Goh WI, Tambichik MA, Iman MA (2018) A review on past and present development on the interlocking loadbearing hollow block (ILHB) system. IOP Conf Ser Earth Environ Sci 140:12135

Boulbes RJ (2020) Troubleshooting finite-element modeling with Abaqus: with application in structural engineering analysis/Raphael Jean Boulbes. Springer, Cham

Casapulla C, Mousavian E, Zarghani M (2019) A digital tool to design structurally feasible semi-circular masonry arches composed of interlocking blocks. Comput Struct 221:111–126. https://doi.org/10.1016/j.compstruc.2019.05.001

Casapulla C, Mousavian E, Argiento L, Ceraldi C, Bagi K (2021) Torsion-shear behaviour at the interfaces of rigid interlocking blocks in masonry assemblages: experimental investigation and analytical approaches. Mater Struct. https://doi.org/10.1617/s11527-021-01721-x

Central Wheatbelt Visitor Centre (2016) Meckering. https://www.wheatbelttourism.com/where-to-stay/meckering/

Chen S, Bagi K (2020) Crosswise tensile resistance of masonry patterns due to contact friction. Proc R Soc A 476:20200439. https://doi.org/10.1098/rspa.2020.0439

Chen XM, Duan J, Qi H, Li YG (2014) Rayleigh damping in Abaqus/explicit dynamic analysis. AMM 627:288–294. https://doi.org/10.4028/www.scientific.net/AMM.627.288

Chopra AK, Chintanapakdee C (2001) Comparing response of SDF systems to near-fault and far-fault earthquake motions in the context of spectral regions. Earthq Eng Struct Dyn 30:1769–1789. https://doi.org/10.1002/eqe.92

Chopra AK (2014) Dynamics of structures: theory and applications to earthquake engineering/Anil K. Chopra, University of California at Berkeley. Prentice-Hall international series in civil engineering and engineering mechanics. Pearson, Boston

Concrete Masonry Association of Australia (2019) Concrete masonry—handbook. https://www.cmaa.com.au/Technical/Manuals/DownloadManual/1?ManualName=CMAA-CM01-2019.pdf

Dassault Systèmes (2022) Abaqus Documentation R2022x. http://help.3ds.com/

DeJong MJ (2009) Seismic assessment strategies for masonry structures. PhD, Massachusetts Institute of Technology

Dell'Endice A, Iannuzzo A, DeJong MJ, van Mele T, Block P (2021) Modelling imperfections in unreinforced masonry structures: discrete element simulations and scale model experiments of a pavilion vault. Eng Struct 228:111499. https://doi.org/10.1016/j.engstruct.2020.111499

Dyskin AV, Pasternak E, Estrin Y (2012) Mortarless structures based on topological interlocking. Front Struct Civ Eng. https://doi.org/10.1007/s11709-012-0156-8

Edwards M, Griffith M, Wehner M, Lam N, Corby N, Jakab M, Habili N (2010) The Kalgoorlie earthquake of the 20th April 2010: preliminary damage survey outcomes. In: Proceedins of 2010 AEES conference. Australian Earthquake Engineering Society, Perth

Elvin A, Uzoegbo HC (2011) Response of a full-scale dry-stack masonry structure subject to experimentally applied earthquake loading. J S Afr Inst Civ Eng 53:22–32

Eurocode 8 (1998) Design of structures for earthquake resistance: part 1: general rules, seismic actions and rules for buildings

Fay L, Cooper P, de Morais HF (2014) Innovative interlocked soil–cement block for the construction of masonry to eliminate the settling mortar. Constr Build Mater 52:391–395. https://doi.org/10.1016/j.conbuildmat.2013.11.030

Ferreira TM, Costa AA, Costa A (2015) Analysis of the out-of-plane seismic behavior of unreinforced masonry: a literature review. Int J Archit Herit 9:949–972. https://doi.org/10.1080/15583058.2014.885996

Ferretti E, Pascale G (2019) Some of the latest active strengthening techniques for masonry buildings: a critical analysis. Materials (basel). https://doi.org/10.3390/ma12071151

GR-63-CORE (1995) Network equipment-building system (NEBS) requirements. Telcordia Technologies, Piscataway

Gupta P, Sankhla SS (2018) A review study on performance of stone masonry building under earthquake. Int J Adv Eng Res Dev 5:45–50. https://doi.org/10.21090/IJAERD.16754

Joint Standards Australia/Standard New Zealand Committee BD-006, General Design Requirements and Loading on Structures (2007) AS 1170.4-2007: structural design actions. Part 4: earthquake actions in Australia, 2nd edn. Australian standard, AS 1170.4-2007. Standards Australia, Sydney

Haener J (1987) Interlocking building block (4,640,071)

Hendry AW (1998) Structural masonry. Macmillan Education UK, London

Hibbitt D, Karlsson B, Sorensen P (2019) Abaqus FEA. Abaqus/Explicit. Dassault Systèmes

Housner GW (1963) The behavior of inverted pendulum structures during earthquakes. Bull Seismol Soc Am 53:403–417

Housner GW, Hudson DE (1958) The Port Hueneme earthquake of March 18, 1957. Bull Seismol Soc Am 48:163–168. https://doi.org/10.1785/BSSA0480020163

Kallioras S, Guerrini G, Tomassetti U, Marchesi B, Penna A, Graziotti F, Magenes G (2018) Experimental seismic performance of a full-scale unreinforced clay-masonry building with flexible timber diaphragms. Eng Struct 161:231–249. https://doi.org/10.1016/j.engstruct.2018.02.016

Kateiva GA (1970) The effects of the meckering earthquake on engineered brick structures in Perth, Western Australia. In: West HW, Speed KH (eds) SIBMAC PROCEEDINGS: proceedings of the second internationai brick masonry conference held in stoke-on-trent, England, on April 12–15, 1970. The British Ceramic Research Association, Stoke-on-Trent, pp 365–368

Liu H, Liu P, Lin K, Zhao S (2016) Cyclic Behavior of Mortarless Brick Joints with Different Interlocking Shapes. Materials (basel). https://doi.org/10.3390/ma9030166

Lourenço PB, Avila L, Vasconcelos G, Alves JP, Mendes N, Costa AC (2013) Experimental investigation on the seismic performance of masonry buildings using shaking table testing. Bull Earthq Eng 11:1157–1190. https://doi.org/10.1007/s10518-012-9410-7

Lubliner J, Oliver J, Oller S, Oñate E (1989) A plastic-damage model for concrete. Int J Solids Struct 25:299–326. https://doi.org/10.1016/0020-7683(89)90050-4

Magenes G, Penna A (2011) Seismic design and assessment of masonry buildings in Europe: recent research and code development issues. In: Ingham JM, Dhanasekar M, Masia M (eds) Proceedings of the 9th Australasian Masonry Conference: Queenstown, New Zealand, 15–18 February 2011. Australasian Masonry Conference, Auckland, NZ

Magenes G, Calvi GM (1997) In-plane seismic response of brick masonry walls. Earthq Eng Struct Dyn 26:1091–1112. https://doi.org/10.1002/(SICI)1096-9845(199711)26:11%3c1091:AID-EQE693%3e3.0.CO;2-6

Malhotra PK (1999) Response of buildings to near-field pulse-like ground motions. Earthq Eng Struct Dyn 28:1309–1326. https://doi.org/10.1002/(SICI)1096-9845(199911)28:11%3c1309:AID-EQE868%3e3.0.CO;2-U

Maqsood T, Edwards M, Ioannou I, Kosmidis I, Rossetto T, Corby N (2016) Seismic vulnerability functions for Australian buildings by using GEM empirical vulnerability assessment guidelines. Nat Hazards 80:1625–1650. https://doi.org/10.1007/s11069-015-2042-x

Martínez M, Atamturktur S, Ross B, Thompson J (2018) Assessing the compressive behavior of dry-stacked concrete masonry with experimentally informed numerical models. J Struct Eng 144:4018080. https://doi.org/10.1061/(ASCE)ST.1943-541X.0002056

Ministry of Housing and Urban-Rural Development of the People's of China (2016) Code for Design of Concrete Structures. GB50010 2010 (2015 Edition). China Architecture Publishing & Media Co., Ltd., Beijing

Ohi K, Takanashi K, Honma Y (1991) Energy input rate spectra of earthquake ground motions. J Struct Constr Eng 420:1–7

Oikonomopoulou F, Bristogianni T, Barou L, Jacobs E, Frigo G, Veer F, Nijsse R (2018) Interlocking cast glass components, exploring a demountable dry-assembly structural glass system. Heron 63:103–138

Oyebisi S (2018) Comparative study of corncob ash-based lateritic interlocking and sandcrete hollow blocks. Geomate. https://doi.org/10.21660/2018.51.45918

Page AW (1991) The behaviour of unreinforced masonry in the Newcastle earthquake. In: Mauerwerksbau DGF (ed) Brick and block masonry. Proceedings of 9th international brick and block masonry conference, vol 2. Deutsche Gesellschaft für Mauerwerksbau eV, Bonn, pp 921–928

Page AW (2019) The Newcastle earthquake and the masonry structures code AS3700. In: Proceedings of 2019 AEES conference. Australian Earthquake Engineering Society, Newcastle

Pan X, Zheng Z, Wang Z (2017) Amplification factors for design of nonstructural components considering the near-fault pulse-like ground motions. Bull Earthq Eng 15:1519–1541. https://doi.org/10.1007/s10518-016-0031-4

Peirs G (1998) Masonry in the third millennium. In: West H, British Masonry Society (eds) Masonry (8): proceedings of the 5th international masonry conference, vol 8. British Masonry Society, pp 6–8

Peña F, Lourenço PB, Mendes N, Oliveira DV (2010) Numerical models for the seismic assessment of an old masonry tower. Eng Struct 32:1466–1478. https://doi.org/10.1016/j.engstruct.2010.01.027

Priestley MJ, Evison RJ, Carr AJ (1978) Seismic response of structures free to rock on their foundations. Bull N Zeal Natl Soc Earthq Eng 11:141–150

Qu B, Stirling BJ, Jansen DC, Bland DW, Laursen PT (2015) Testing of flexure-dominated interlocking compressed earth block walls. Constr Build Mater 83:34–43. https://doi.org/10.1016/j.conbuildmat.2015.02.080

Ramamurthy K, Kunhanandan Nambiar EK (2004) Accelerated masonry construction review and future prospects. Prog Struct Eng Mater 6:1–9. https://doi.org/10.1002/pse.162

Rawling T (2012) The Victorian earthquake didn't do much damage… but the next one might. https://theconversation.com/the-victorian-earthquake-didnt-do-much-damage-but-the-next-one-might-7787

Shahi SK, Baker JW (2014) An efficient algorithm to identify strong-velocity pulses in multicomponent ground motions. Bull Seismol Soc Am 104:2456–2466. https://doi.org/10.1785/0120130191

Shahi SK, Baker JW (2019) Erratum to an efficient algorithm to identify strong-velocity pulses in multicomponent ground motions. Bull Seismol Soc Am 109:2767. https://doi.org/10.1785/0120190236

Shi T, Zhang X, Hao H, Chen C (2021a) Experimental and numerical investigation on the compressive properties of interlocking blocks. Eng Struct 228:111561. https://doi.org/10.1016/j.engstruct.2020.111561

Shi T, Zhang X, Hao H, Xie G (2021b) Experimental and numerical studies of the shear resistance capacities of interlocking blocks. J Build Eng 44: https://doi.org/10.1016/j.jobe.2021.103230

Smith IC (1969) Notes on the meckering earthquake. N Z Eng 24:221–224

Somerville P, Graves R (1993) Conditions that give rise to unusually large long period ground motions. Struct Design Tall Build 2:211–232. https://doi.org/10.1002/tal.4320020304

Sorrentino L, AlShawa O, Decanini LD (2011) The relevance of energy damping in unreinforced masonry rocking mechanisms. Experimental and analytic investigations. Bull Earthq Eng 9:1617–1642. https://doi.org/10.1007/s10518-011-9291-1

Structural Engineering Institute; American Society of Civil Engineers, publisher (2017) ASCE 7–16: minimum design loads and associated criteria for buildings and other structures. ASCE/SEI, 7–16. American Society of Civil Engineers, Reston, Virginia

Sturm T, Ramos LF, Lourenço PB (2015) Characterization of dry-stack interlocking compressed earth blocks. Mater Struct 48:3059–3074. https://doi.org/10.1617/s11527-014-0379-3
Sucuoglu H, McNiven HD (1991) Seismic shear capacity of reinforced masonry piers. J Struct Eng 117:2166–2185. https://doi.org/10.1061/(ASCE)0733-9445(1991)117:7(2166)
Sun B, Yan P, Hu C, Zhang M (2008) Overview on seismic damage to different structures in Yingxiu Town during Wenchuan Earthquake. J Earthq Eng Eng Vib 28:1–9. https://doi.org/10.13197/j.eeev.2008.05.002
Thanoon WA, Jaafar MS, Abdul Kadir MR, Abang Ali AA, Trikha D, Najm AM (2004) Development of an innovative interlocking load bearing hollow block system in Malaysia. Constr Build Mater 18:445–454. https://doi.org/10.1016/j.conbuildmat.2004.03.013
Tomaževič M (1999) Earthquake-resistant design of masonry buildings. Series in innovations in structures and construction, vol 1. Imperial College Press, London
Turek ME (2002) In-plane shake-table testing of unreinforced masonry walls strengthened with fibre reinforced-plastics. The University of British Columbia, Master
Turek M, Ventura CE, Kuan S (2007) In-plane shake-table testing of GFRP-strengthened concrete masonry walls. Earthq Spectra 23:223–237. https://doi.org/10.1193/1.2429564
Uang C-M, Bertero VV (1990) Evaluation of seismic energy in structures. Earthq Eng Struct Dyn 19:77–90. https://doi.org/10.1002/eqe.4290190108
University of California, Berkeley (2021) Pacific Earthquake Engineering Research Center (PEER) Ground Motion Database: NGA-West2 ground motion database. https://ngawest2.berkeley.edu/spectras/new?sourceDb_flag=1
Wang Z, Yu Z (2004) Concrete damage model based on energy loss. J Build Mater 7:365–369
Wang G, Li Y, Zheng N, Ingham JM (2017) Testing and modelling the in-plane seismic response of clay brick masonry walls with boundary columns made of precast concrete interlocking blocks. Eng Struct 131:513–529. https://doi.org/10.1016/j.engstruct.2016.10.035
Wehner M, Edwards M, Corby N (2010) Survey of Kalgoorlie earthquake damage. Geoscience Australia, Kalgoorlie
Xie G, Zhang X, Hao H, Thomas J (2020) Response of Mortar-Free Interlocking Brick Wall under Seismic Excitation. In: Proceedings of 2020 Australian Earthquake Engineering Society Conference, pp 309–316
Zhang QW (2007) Statistical damage identification for bridges using ambient vibration data. Comput Struct 85:476–485. https://doi.org/10.1016/j.compstruc.2006.08.071
Zhang X, Hao H, Li C (2017) The effect of concrete shear key on the performance of segmental columns subjected to impact loading. Adv Struct Eng 20:352–373. https://doi.org/10.1177/1369433216650210
Zhang X, Hao H, Li C, van Do T (2018) Experimental study on the behavior of precast segmental column with domed shear key and unbonded Post-Tensioning tendon under impact loading. Eng Struct 173:589–605. https://doi.org/10.1016/j.engstruct.2018.07.002
Zhang X, Hao H, Zheng J, Hernandez F (2021) The mechanical performance of concrete shear key for prefabricated structures. Adv Struct Eng 24:291–306. https://doi.org/10.1177/1369433220950618
Zhang C, Lu J, Jia H, Lai Z, Li X, Wang P (2020) Influence of near-fault ground motion characteristics on the seismic response of cable-stayed bridges. Bull Earthq Eng 18:6375–6403. https://doi.org/10.1007/s10518-020-00926-9

Terms and Conditions

Springer Nature journal content, brought to you courtesy of Springer Nature Customer Service Center GmbH ("Springer Nature").

Springer Nature supports a reasonable amount of sharing of research papers by authors, subscribers and authorised users ("Users"), for small-scale personal, non-commercial use provided that all copyright, trade and service marks and other proprietary notices are maintained. By accessing, sharing, receiving or otherwise using the Springer Nature journal content you agree to these terms of use ("Terms"). For these purposes, Springer Nature considers academic use (by researchers and students) to be non-commercial.

These Terms are supplementary and will apply in addition to any applicable website terms and conditions, a relevant site licence or a personal subscription. These Terms will prevail over any conflict or ambiguity with regards to the relevant terms, a site licence or a personal subscription (to the extent of the conflict or ambiguity only). For Creative Commons-licensed articles, the terms of the Creative Commons license used will apply.

We collect and use personal data to provide access to the Springer Nature journal content. We may also use these personal data internally within ResearchGate and Springer Nature and as agreed share it, in an anonymised way, for purposes of tracking, analysis and reporting. We will not otherwise disclose your personal data outside the ResearchGate or the Springer Nature group of companies unless we have your permission as detailed in the Privacy Policy.

While Users may use the Springer Nature journal content for small scale, personal non-commercial use, it is important to note that Users may not:

1. use such content for the purpose of providing other users with access on a regular or large scale basis or as a means to circumvent access control;
2. use such content where to do so would be considered a criminal or statutory offence in any jurisdiction, or gives rise to civil liability, or is otherwise unlawful;
3. falsely or misleadingly imply or suggest endorsement, approval , sponsorship, or association unless explicitly agreed to by Springer Nature in writing;
4. use bots or other automated methods to access the content or redirect messages
5. override any security feature or exclusionary protocol; or
6. share the content in order to create substitute for Springer Nature products or services or a systematic database of Springer Nature journal content.

In line with the restriction against commercial use, Springer Nature does not permit the creation of a product or service that creates revenue, royalties, rent or income from our content or its inclusion as part of a paid for service or for other commercial gain. Springer Nature journal content cannot be used for inter-library loans and librarians may not upload Springer Nature journal content on a large scale into their, or any other, institutional repository.

These terms of use are reviewed regularly and may be amended at any time. Springer Nature is not obligated to publish any information or content on this website and may remove it or features or functionality at our sole discretion, at any time with or without notice. Springer Nature may revoke this licence to you at any time and remove access to any copies of the Springer Nature journal content which have been saved.

To the fullest extent permitted by law, Springer Nature makes no warranties, representations or guarantees to Users, either express or implied with respect to the Springer nature journal content and all parties disclaim and waive any implied warranties or warranties imposed by law, including merchantability or fitness for any particular purpose.

Please note that these rights do not automatically extend to content, data or other material published by Springer Nature that may be licensed from third parties.

If you would like to use or distribute our Springer Nature journal content to a wider audience or on a regular basis or in any other manner not expressly permitted by these Terms, please contact Springer Nature at

onlineservice@springernature.com